Scottish Universities Environmental Research Centre

Luminescence Measurements of Sediment Cores from Lake Esmeralda and Monolith Lake, James Ross Island Archipelago

December 2017

David Sanderson[1], Alan Cresswell[1], Matěj Roman[2], Anna Píšková[3], Kateřina Kopalová[3], Daniel Nývlt[4], Juan Manuel Lirio[5]

[1]SUERC, East Kilbride, Glasgow
[2]Department of Physical Geography and Geoecology, Faculty of Science, Charles University, Prague, Czechia
[3]Department of Ecology, Faculty of Science, Charles University, Prague, Czechia;
[4]Department of Geography, Faculty of Science, Masaryk University, Brno, Czechia
[5]Instituto Antártico Argentino, Buenos Aires, Argentina

East Kilbride Glasgow G75 0QF Telephone: 01355 223332 Fax: 01355 229898

Summary

The James Ross Island archipelago is located at the northern end of the Antarctic Peninsula, one of the most sensitive regions to global climate changes. The islands are characterised by large deglaciated areas containing remarkable sedimentary archives, including lacustrine sediments, which record past climatic conditions. Sedimentary sequences from two lakes in the area have been retrieved for multi-proxy analyses of sediment properties to reconstruct the past climatic and environmental evolution. This data needs to be set into a reliable chronological framework to correlate the environmental records with other regional palaeoreconstructions from ice cores, marine sediments and glacial chronologies. There are large uncertainties in radiocarbon chronologies ensuing from large reservoir effects and the scarcity of terrestrial macroremains. Luminescence dating techniques, which measure ages of commonly occurring minerals, could therefore provide a robust chronology and offer new insights into the age and mode of sediment deposition. Previous studies of Antarctic lacustrine sediments have shown large residual thermoluminescence (TL) signals, and smaller residual infra-red stimulated luminescence (IRSL) signals. Optically stimulated luminescence (OSL) has been applied to samples from raised Antarctic lake deltas and shorelines, and sediments from subglacial lakes.

Sedimentary cores were collected from Lake Esmeralda (Vega Island) and Monolith Lake (James Ross Island), with one core from each lake examined in this work. Luminescence profiling has been conducted on the two cores, with measurements on bulk sediments using the SUERC Portable OSL instrument under blue and IR stimulation, and laboratory profiling using IRSL and TL on separated 90-250 µm polymineral grains and OSL on 90-250 µm quartz grains. The profile measurements show significant differences in estimated stored dose between methods, with the OSL giving the lowest doses, followed by IRSL and TL, consistent with previous studies showing large residual signals in TL and smaller residuals in some IRSL measurements. Quantitative OSL analyses were conducted on 150-250 µm quartz grains extracted from selected samples from these cores to calculate sedimentary ages.

For Lake Esmeralda, the ages show a general increase with depth, from 0.4 to 0.8 ka, with some small age inversions between 40 and 50 cm and between 140 and 150 cm.

For Monolith Lake, the top 5 cm cover an age range similar to the entire length of the Lake Esmeralda core and show significantly lower luminescence sensitivity. Below 5 cm there is a significant increase in apparent age, to 2.5-3.0 ka, which is approximately constant within ~0.5 ka for most of the core, and increased sensitivity. The lower samples below 26 cm are significantly younger and form a progression of older aged material at greater depth. This suggests that within the last 1000 years there has been a significant change in the sediment supply to Monolith Lake. The age profile for Monolith Lake, in particular the younger ages for material below 26 cm, suggests that the sediments below 5 cm carried a residual dose when they were deposited in the lake, with the deepest sediments in the core carrying a smaller residual, or even having being reset and thus giving a true age for these layers. The larger doses measured by IRSL and TL in the profiling indicate that it is likely that the luminescence centres associated with these signals carried a residual dose for all samples. Further exploration of these signals may reveal additional information on the sediment histories.

Contents

Summary i
1. Introduction 1
2. Methods 4
2.1. Sampling and sample preparation 4
2.2. Portable OSL Reader Measurements 4
2.3. Laboratory calibrated screening measurements 5
2.4. Dosimetry Sample Preparation 5
2.5. Quartz SAR luminescence measurements 6
3. Results 8
3.1. Portable OSL Instrument Results 8
3.2. Laboratory Profiling Results 9
3.3. Laboratory Dosimetry Results 11
3.4. Quartz single aliquot equivalent dose determinations 13
3.5. Scanning Electron Microscopy 16
4. Discussion and conclusions 18
5. References 20
Appendix A: Water content measurements 21
Appendix B: Profiling Results 22
Appendix C: Dose response curves 29
Appendix D: Dose Distribution Plots 34
Appendix E. Tabulated age-depth relationships 47

List of figures

Figure 1.1 Location of the studied area within the Antarctic Peninsula region and James Ross Island Archipelago. Bathymetric map of Lake Esmeralda with denoted coring locations and general view of Lake Esmeralda with its catchment and surroundings. 2
Figure 1.2 Lithological description of MON1B core (parallel to MON1A core) from Monolith Lake, depicted on the aerial picture with inflow and outflow streams and hyaloclastite breccia boulders. 3
Figure 3.1: Portable IRSL/OSL reader results of ESM3/14 samples (SUTL2959) plotted versus sediment depth. 8
Figure 3.2: Portable IRSL/OSL reader results of MON1A samples (SUTL2960) plotted versus sediment depth and water content (in %). 8
Figure 3.3: Laboratory profiling results for SUTL2959, showing sensitivity for the three measurements (left) the change in sensitivity over the cycle (centre) and estimated stored dose (right). 9
Figure 3.4: Laboratory profiling results for SUTL2960, showing sensitivity for the three measurements (left) the change in sensitivity over the cycle (centre) and estimated stored dose (right). 10
Figure 3.5: Age depth profiles for the Lake Esmeralda core (SUTL2959, ESM-3) and Monolith Lake core (SUTL2960, MON-1A). Showing ages determined from SAR OSL measurements (red) and apparent ages from the profile measurements (blue). .. 16
Figure 3.6: Example SEM spectra from SUTL2960/5, 2960/15 and 2960/27. 17
Figure C.1: Dose response curve for SUTL2959/1, average for all accepted aliquots. 29
Figure C.2: Dose response curve for SUTL2959/2, average for all accepted aliquots. 29
Figure C.3: Dose response curve for SUTL2959/3, average for all accepted aliquots. 29
Figure C.4: Dose response curve for SUTL2959/4, average for all accepted aliquots. 30
Figure C.5: Dose response curve for SUTL2959/5, average for all accepted aliquots. 30
Figure C.6: Dose response curve for SUTL2959/6, average for all accepted aliquots. 30
Figure C.7: Dose response curve for SUTL2959/7, average for all accepted aliquots. 31
Figure C.8: Dose response curve for SUTL2959/8, average for all accepted aliquots. 31
Figure C.9: Dose response curve for SUTL2959/9, average for all accepted aliquots. 31
Figure C.10: Dose response curve for SUTL2960/2, average for all accepted aliquots. 32
Figure C.11: Dose response curve for SUTL2960/5, average for all accepted aliquots. 32
Figure C.12: Dose response curve for SUTL2960/15, average for all accepted aliquots. 32
Figure C.13: Dose response curve for SUTL2960/27, average for all accepted aliquots. 33
Figure D.1: Radial plot for SUTL2959/1. The line indicates the weighted mean. 34

Figure D.2: Probability distribution plot for SUTL2959/1. The dashed line indicates the weighted mean. 34
Figure D.3: Radial plot for SUTL2959/2. The line indicates the robust mean. 35
Figure D.4: Probability distribution plot for SUTL2959/2. The dashed line indicates the robust mean. 35
Figure D.5: Radial plot for SUTL2959/3. The black line indicates the weighted mean, with the grey line indicating the robust mean. 36
Figure D.6: Probability distribution plot for SUTL2959/3. The dashed line indicates the weighted mean. 36
Figure D.7: Radial plot for SUTL2959/4. The line indicates the weighted mean. 37
Figure D.8: Probability distribution plot for SUTL2959/4. The dashed line indicates the weighted mean. 37
Figure D.9: Radial plot for SUTL2959/5. The line indicates the robust mean. 38
Figure D.10: Probability distribution plot for SUTL2959/5. The dashed line indicates the robust mean. 38
Figure D.11: Radial plot for SUTL2959/6. The line indicates the weighted mean. 39
Figure D.12: Probability distribution plot for SUTL2959/6. The dashed line indicates the weighted mean. 39
Figure D.13: Radial plot for SUTL2959/7. The line indicates the weighted mean for the lower dose component. 40
Figure D.14: Probability distribution plot for SUTL2959/7. The dashed line indicates the weighted mean for the lowest dose peak. 40
Figure D.15: Abanico plot for SUTL2959/8. The dashed line indicates the weighted mean. 41
Figure D.16: Probability distribution plot for SUTL2959/8. The dashed line indicates the weighted mean. 41
Figure D.17: Radial plot for SUTL2959/9. The dashed line indicates the weighted mean. 42
Figure D.18: Probability distribution plot for SUTL2959/9. The dashed line indicates the weighted mean. 42
Figure D.19: Radial plot for SUTL2960/2. The dashed line indicates the unweighted mean. 43
Figure D.20: Probability distribution plot for SUTL2960/2. The dashed line indicates the unweighted mean. 43
Figure D.21: Radial plot for SUTL2960/5. The dashed line indicates the weighted mean. 44
Figure D.22: Probability distribution plot for SUTL2960/5. The dashed line indicates the weighted mean. 44
Figure D.23: Abanico plot for SUTL2960/15. The dashed line indicates the robust mean. 45
Figure D.24: Probability distribution plot for SUTL2960/15. The dashed line indicates the robust mean. 45
Figure D.25: Radial plot for SUTL2960/27. The dashed line indicates the weighted mean. 46
Figure D.26: Probability distribution plot for SUTL2960/27. The dashed line indicates the weighted mean. 46

List of tables

Table 2.1: Summary of samples and SUERC laboratory reference codes 4
Table 3.1: Activity and equivalent concentrations of K, U and Th determined by HRGS 12
Table 3.2: Infinite matrix dose rates determined by HRGS and TSBC 12
Table 3.3: Effective beta and gamma dose rates following water correction. 13
Table 3.4: SAR quality parameters 14
Table 3.5: Comments on equivalent dose distributions; preferred estimates in bold .. 15
Table 3.6: Quartz OSL ages 15
Table A.1: Measured water contents for the Monolith Lake core (SUTL2960) sections as received (wet) and saturated, with assumed average water content during burial. . 21
Table B.1: Instrumental profiling results for Lake Esmeralda (SUTL2959) 22
Table B.2: Laboratory profiling results for Lake Esmeralda (SUTL2959) 23
Table B.3: Instrumental profiling results for Monolith Lake (SUTL2960) 24
Table B.4: Profiling results for Monolith Lake (SUTL2960) 26
Table E.1: Dose rates, stored doses and ages for the profiling OSL measurements and SAR analysis of SUTL2959 (Lake Esmeralda). 47
Table E.2: Dose rates (measured values in bold, other values interpolated from these), stored doses and ages for the profiling OSL measurements and SAR analysis of SUTL2960 (Monolith Lake). 47

1. Introduction

The Antarctic Peninsula is one of the most sensitive regions to global climate changes, which is evident in the rapid increase of air temperatures over the last ~50 years. The James Ross Island archipelago is at the same time characteristic by large deglaciated areas that contain remarkable sedimentary archives, including lacustrine sediments. In order to elucidate past environmental conditions, we retrieved sedimentary sequences from two lakes in the area and performed multi-proxy analyses of sediment properties. Integration of available proxy data should allow us to reconstruct the past climatic and environmental evolution that needs to be, however, set into a reliable chronological framework. Knowledge of the time of deposition and the sediment age is crucial for correlation of our record with other regional palaeoreconstructions from ice cores, marine sediments and glacial chronologies. Hitherto dated by radiocarbon only, the large uncertainties in chronology ensuing from large ^{14}C reservoir effect and scarcity of terrestrial macroremains call for application of other dating methods. Studies of lake sediments and source materials for lakes in the McMurdo Dry Valleys (Doran et.al. 1999, Berger & Doran 2001) have demonstrated erroneous ^{14}C dates, and shown that thermoluminescence (TL) signals were not fully removed from feldspars surface materials in most cases, and that TL measurements of sediments carried a substantial relic signal. The use of infra-red stimulated luminescence (IRSL) produced an increase in age with depth, but with a residual age of ~600 years. IRSL measurements on samples from the Schirmacher Oasis (Krause et.al. 1997) showed that the plagioclase feldspars used were readily bleached by daylight with stable emissions, applied to sediments >70 ka where a residual similar to that noted by Berger & Doran (2001) would not be significant. Optically stimulated luminescence (OSL) on quartz grains has been successfully applied to samples from raised Antarctic lake margins and deltas (Roberts et.al. 2009, Hodgson et.al. 2009a). Sediments from a former subglacial lake (Hodgson et.al. 2009b) resulted in largely saturated OSL signals, suggesting a large residual for those sediments.

In this work, rapid profiling measurements have been conducted using blue and IR stimulation on bulk materials using a portable OSL reader, and using IRSL and TL on separated polyminerals and OSL on nominal quartz grains. This allows a direct comparison between the different methods on the same material. Quantitative measurements of selected samples using OSL on density separated and acid etched quartz grains have also been undertaken to determine sediment ages.

Two sedimentary cores from Lake Esmeralda, Vega Island, and Monolith Lake, James Ross Island, were recovered. Catchments of both lakes are presently deglaciated and covered by relatively thin (<0.5 m) snow cover in winter months. Both lakes are seasonally ice-free, usually for 2–3 months, and are sufficiently deep so that the bottom waters do not freeze during the winter. Lake Esmeralda is classified as a meromictic, strongly acidic (pH 4.7) lake infilling a depression in Cretaceous sandstones. Sources of allochthonous matter include Tertiary volcanic rocks (hyaloclastite breccias, flood basalts), influx of which was, however, diminished after the main influent stream diverted its flow by river piracy (Fig. 1). Alluvial fans and deltaic deposits in the flat lake basin point to past variations in lake level. Monolith Lake is shallower (depth ~2 m) and the sediments thickness reaches only around 50 cm. However, previous ^{14}C dating suggests their high age, on the order of several

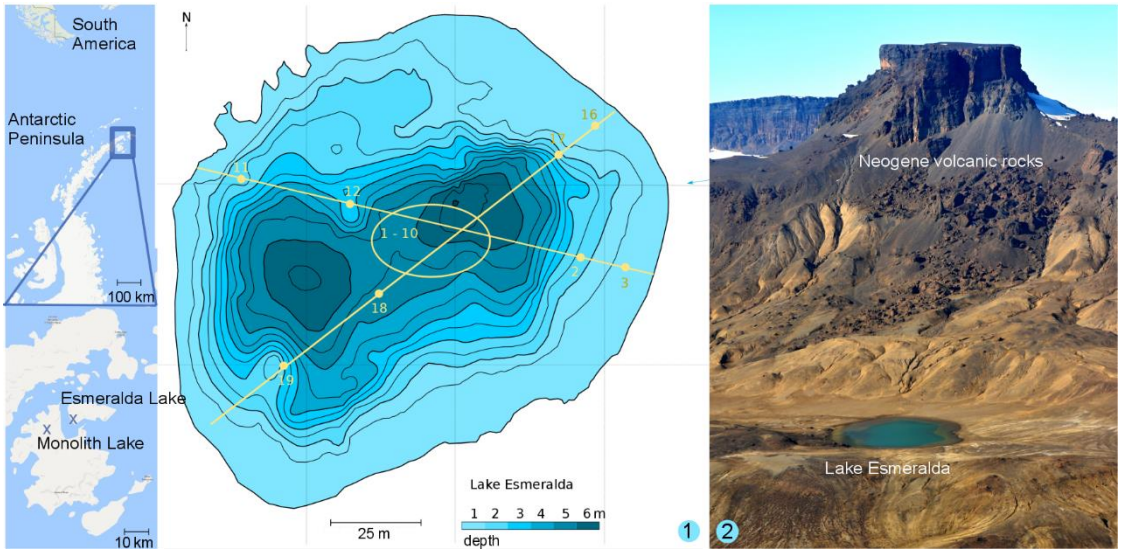

Figure 1.1 Location of the studied area within the Antarctic Peninsula region and James Ross Island Archipelago. Bathymetric map of Lake Esmeralda with denoted coring locations and general view of Lake Esmeralda with its catchment and surroundings.

thousands of years (Björck et al 1996). Monolith Lake is located at an altitude of 55 m a.s.l. and a small tributary from Whiskey Glacier flows into the southern part of the lake (Fig. 1.2).

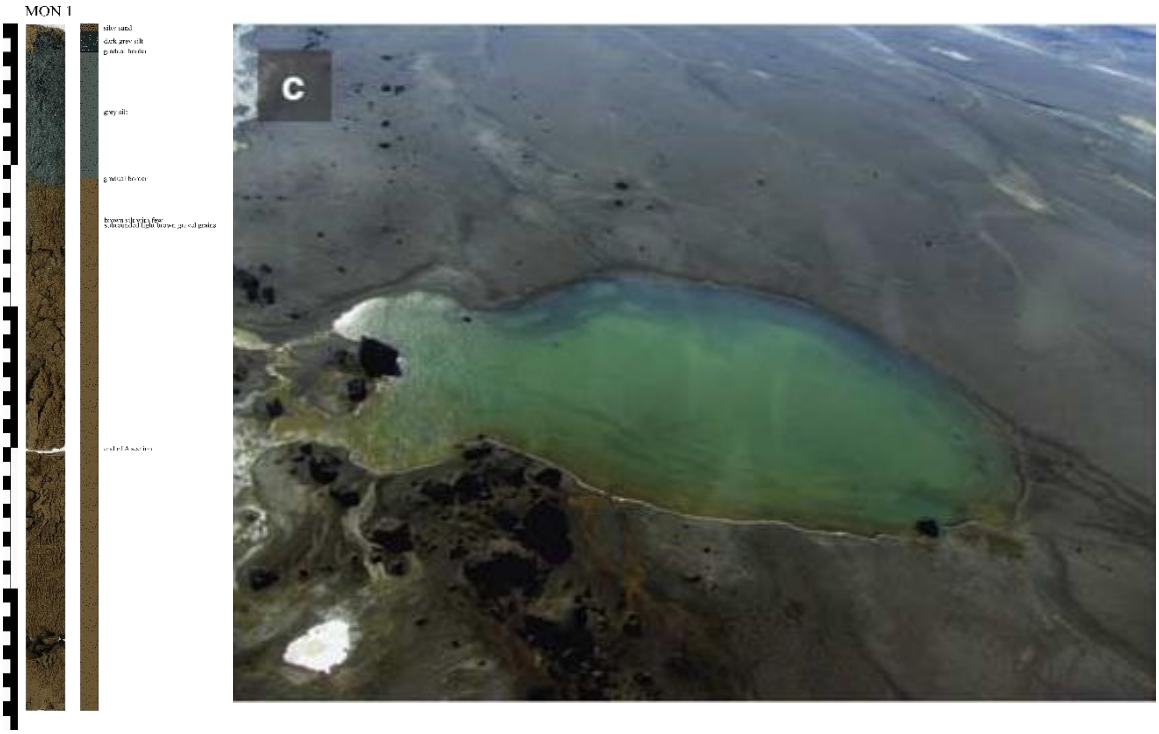

Figure 1.2 Lithological description of MON1B core (parallel to MON1A core) from Monolith Lake, depicted on the aerial picture with inflow and outflow streams and hyaloclastite breccia boulders.

2. Methods

2.1. Sampling and sample preparation

The investigated composite sedimentary core ESM3/14 (SUTL 2959) was recovered from the depocenter (depth ~6 m, Fig. 1.1) by a Russian chamber corer and consists of two nearly 1 m long individual cores linked together by the known depth of coring. The core ESM3/14 is in total 177 cm long, is composed of grey silty sediment and interspersed with dark or ochre laminae and moss remains. Analyses performed on this core include microfossil (especially diatom) determination, magnetic susceptibility, grain size distribution, XRF elemental composition, XRD mineralogical composition, cation exchange capacity and high pressure liquid chromatography.

Core MON1A (SUTL2960) consists of one single coring profile obtained from the depocenter of Monolith Lake during the field season of 2017. The top part of the core (0–10 cm) is composed grey silty sediment with more organic remnants, whereas lowermost part consists of brown clayey silt with occasional findings of subrounded light brown gravel grains (Fig 1.2).

Each sample was given a laboratory (SUTL) reference code upon receipt at SUERC, as summarised in Table 2.1.

SUERC code	Description
SUTL2959/1	ESM3/20, real depth 15.5 cm, wet weight
SUTL2959/2	ESM3/40, real depth 35.5 cm, wet weight
SUTL2959/3	ESM3/60, real depth 54.5 cm, wet weight
SUTL2959/4	ESM3/80, real depth 74.5 cm, wet weight
SUTL2959/5	ESM3/100, real depth 92.5 cm, wet weight
SUTL2959/6	ESM3/120, real depth 111.5 cm, wet weight
SUTL2959/7	ESM3/140, real depth 132.5 cm, wet weight
SUTL2959/8	ESM3/160, real depth 151.5 cm, wet weight
SUTL2959/9	ESM3/180, real depth 171.5 cm, wet weight
SUTL2960/1-31	MON1A core, depth 30 cm, cut in 1-cm steps

Table 2.1: Summary of samples and SUERC laboratory reference codes

2.2. Portable OSL Reader Measurements

All samples were first appraised using the SUERC portable OSL reader, following an interleaved sequence of system dark count (background), infra-red stimulated luminescence (IRSL) and OSL, similar to that described by Sanderson and Murphy (2010). This method allows for the calculation of IRSL and OSL net signal intensities, depletion indices and IRSL:OSL ratios, which are then used to generate luminescence-depth profiles.

2.3. Laboratory calibrated screening measurements

Having established that there are measureable stratigraphic trends in the luminescence 'field' profiles, it remains to be determined whether these signal progressions are influenced, or indeed controlled, by sensitivity variations. Laboratory profiling provides one means to assess luminescence sensitivity distributions, and the first preliminary assessment of apparent doses.

All profiling samples were wet sieved at 90 and 250 μm. The 90-250 μm fractions were then subjected to acid treatments of 1M HCl for 30 mins, 15% HF for 5mins and 1M HCl for 10mins. The samples were split into two fractions, one for polymineral analysis and one for quartz analysis. The quartz fraction was submitted to further acid treatments of 40% HF for 40mins and 1M HCl for 10mins.

Luminescence sensitivities (Photon Counts per Gy) and stored doses (Gy) were evaluated from paired aliquots of the polymineral and HF-etched quartz fractions, using Risø DA-15 automatic readers (following procedures established in Burbidge et al., 2007; Sanderson et al., 2001; Sanderson et al., 2003). For the quartz samples, the readout cycle consisted of a 10s preheat at 200°C with a 30s OSL measurements using the blue LEDs at 125°C. These measurements were conducted for the natural signal and following 5 Gy and 50 Gy, with a repeat of the 5 Gy, regenerative doses each followed by readout cycles for a nominal 1 Gy test dose. For the polymineral samples, the 200˚C preheat was followed by 30s OSL measurements using the IR LEDs at 50˚C and a TL measurement to 500˚C, for the natural signal and the 5 Gy, 50 Gy and repeat 5 Gy regenerative doses without a test dose cycle.

For OSL and IRSL measurements net counts were determined for each sample by summing counts in the first 40 channels (5 s) of each measurement and subtracting the counts in the final 40 channels. For TL measurements, the gross count in the 300-500°C was determined for each measurement.

2.4. Dosimetry Sample Preparation

For SUTL2959 the material was dried prior to transport to SUERC. Depending on quantity of material available for each section 10g or 20g of dried material was removed for laboratory dosimetry measurements. SUTL2960 was frozen for transport, and defrosted and sectioned at SUERC. The sections were weighed, saturated with water and re-weighed. Following oven drying at 50 °C to constant weight, the actual and saturated water contents were determined as fractions of dry weight. These data were used, together with information on field conditions to determine water contents and an associated water content uncertainty for use in dose rate determination. The dried material for SUTL2960 has been retained for dosimetry and further luminescence analysis at a future date.

Beta dose rates were measured directly using the SUERC TSBC system (Sanderson, 1988). Count rates were determined with six replicate 300 s counts on each sample, bracketed by background measurements and sensitivity determinations using the Shap Granite secondary reference material. Infinite-matrix dose rates were calculated by scaling the net count rates of samples and reference material to the working beta dose

rate of the Shap Granite (6.25 ± 0.03 mGy a^{-1}). The estimated errors combine counting statistics, observed variance and the uncertainty on the reference value. These dried materials were transferred to plastic petri dishes and sealed with epoxy resin for high-resolution gamma spectrometry (HRGS). Each pot was stored for 3 weeks prior to measurement to allow equilibration of ^{222}Rn daughters.

HRGS measurements were performed using a 50% relative efficiency "n" type hyper-pure Ge detector (EG&G Ortec Gamma-X) operated in a low background lead shield with a copper liner. Gamma ray spectra were recorded over the 30 keV to 3 MeV range from each sample, interleaved with background measurements and measurements from SUERC Shap Granite standard in the same geometries. Sample counts were for 80 ks. The spectra were analysed to determine count rates from the major line emissions from ^{40}K (1461 keV), and from selected nuclides in the U decay series (^{234}Th, ^{226}Ra + ^{235}U, ^{214}Pb, ^{214}Bi and ^{210}Pb) and the Th decay series (^{228}Ac, ^{212}Pb, ^{208}Tl) and their statistical counting uncertainties. Net rates and activity concentrations for each of these nuclides were determined relative to Shap Granite by weighted combination of the individual lines for each nuclide. The internal consistency of nuclide specific estimates for U and Th decay series nuclides was assessed relative to measurement precision, and weighted combinations used to estimate mean activity concentrations (Bq kg^{-1}) and elemental concentrations (% K and ppm U, Th) for the parent activity. These data were used to determine infinite matrix dose rates for alpha, beta and gamma radiation.

The dose rate measurements were used in combination with the assumed burial water contents, to determine the overall effective dose rates for age estimation. Cosmic dose rates were evaluated by combining latitude and altitude specific dose rates (0.185 ± 0.010 mGy a^{-1}) for the site with corrections for estimated depth of overburden using the method of Prescott and Hutton (1994).

2.5. Quartz SAR luminescence measurements

All measurements were conducted using a Risø DA-15 automatic reader equipped with a ^{90}Sr/^{90}Y β-source for irradiation, blue LEDs emitting around 470 nm and infrared (laser) diodes emitting around 830 nm for optical stimulation, and a U340 detection filter pack to detect in the region 270-380 nm, while cutting out stimulating light (Bøtter-Jensen et al., 2000).

Equivalent dose determinations were made on sets of 16 aliquots per sample, using a single aliquot regeneration (SAR) sequence (cf Murray and Wintle, 2000). Using this procedure, the OSL signal levels from each individual disc were calibrated to provide an absorbed dose estimate (the equivalent dose) using an interpolated dose-response curve, constructed by regenerating OSL signals by beta irradiation in the laboratory. Sensitivity changes which may occur as a result of readout, irradiation and preheating (to remove unstable radiation-induced signals) were monitored using small test doses after each regenerative dose. Each measurement was standardised to the test dose response determined immediately after its readout, to compensate for changes in sensitivity during the laboratory measurement sequence. The regenerative doses were chosen to encompass the likely value of the equivalent (natural) dose. A repeat dose point was included to check the ability of the SAR procedure to correct for laboratory-induced sensitivity changes (the 'recycling test'), a zero dose point is included late in

the sequence to check for thermally induced charge transfer during the irradiation and preheating cycle (the ‘zero cycle’), and an IR response check included to assess the magnitude of non-quartz signals. Based on the profiling measurements, the expected range of stored doses was approximately 0-10 Gy, so regenerative dose response curves were constructed using doses of 1.0, 2.0, 5.0, 10.0 and 20.0 Gy, with test doses of 1.0 Gy. The 16 aliquot sets were sub-divided into four subsets of four aliquots, such that four preheating regimes were explored (200°C, 220°C, 240°C and 260°C).

3. Results

3.1. Portable OSL Instrument Results

The data from the profile measurements on SUTL2959 (ESM3) are shown in Fig 3.1. These results confirm that both IRSL and OSL produce measurable signals, with local maxima in the intensities and depletion ratios of both at 20 cm and 120-140 cm depth. These variations in depth may reflect changing luminescence sensitivities, dose rates or sedimentation rates.

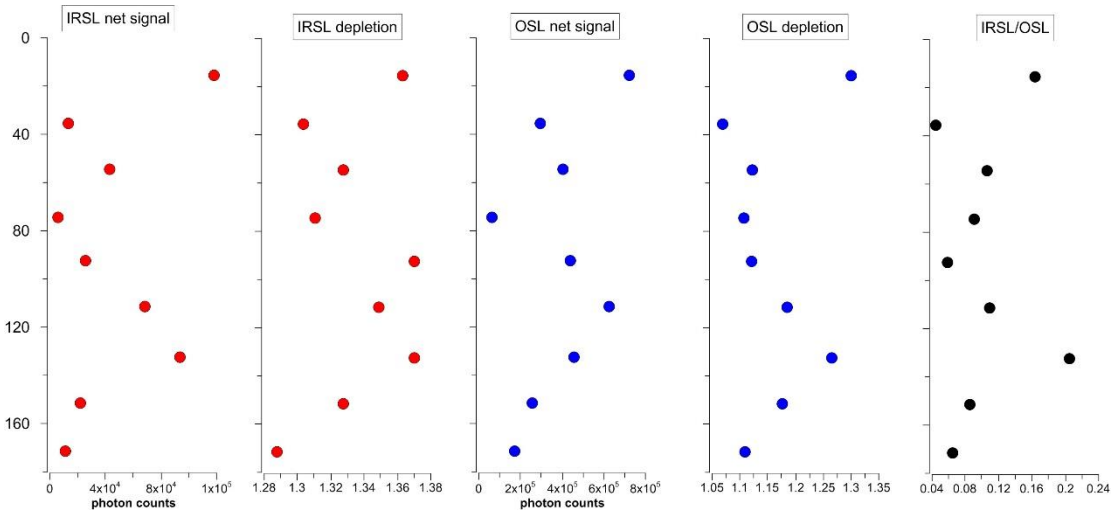

Figure 3.1: Portable IRSL/OSL reader results of ESM3/14 samples (SUTL2959) plotted versus sediment depth.

The data from the profile measurements on SUTL2960 (MON1A) are shown in Fig 3.2, along with measured water content. It can be seen that both the IRSL and OSL net signals increase over the first 10 cm, then form a plateau before increasing more slowly from about 25 cm down the core.

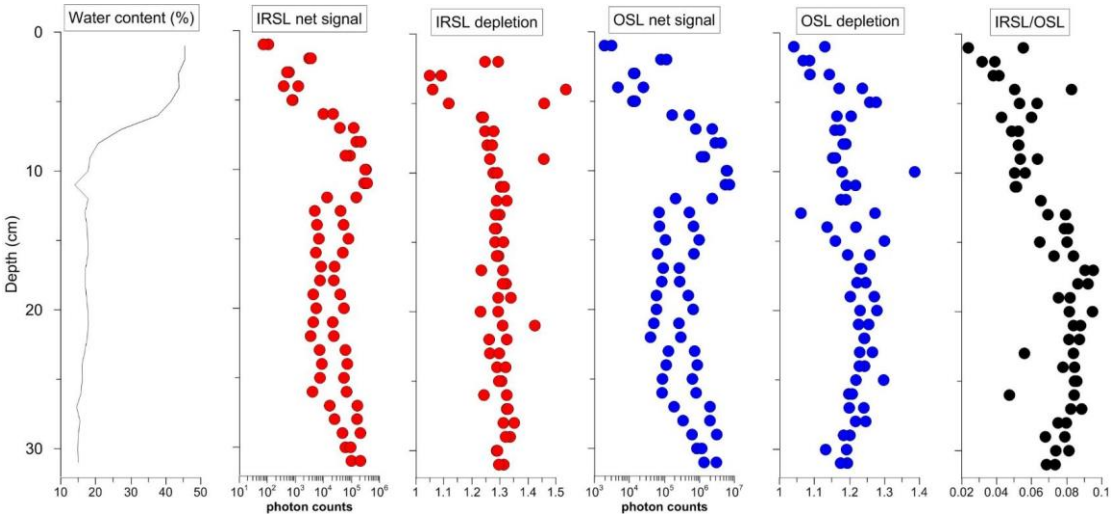

Figure 3.2: Portable IRSL/OSL reader results of MON1A samples (SUTL2960) plotted versus sediment depth and water content (in %).

3.2. Laboratory Profiling Results

The laboratory profiling results for SUTL2959 (ESM3) are shown in Fig 3.3, with the sensitivity, sensitivity change and estimated stored dose for the OSL (on the quartz fractions) and IRSL and TL (both on the polymineral fractions). For all samples the TL is the most sensitive method, followed by the IRSL and OSL, with little variation with depth. The sensitivity change for the TL and IRSL (the ratio of counts following the second 5 Gy irradiation to the counts following the first) is close to unity, whereas the sensitivity change for the OSL (the ratio of counts following the second 1 Gy TD to the counts following the first TD) varies significantly from unity with most samples showing a sensitivity increase. The estimated stored doses from OSL and IRSL generally increase slightly down the core, with the IRSL values approximately 5x greater than the OSL. The estimated stored doses from the TL measurements are very much higher, and approximately constant down the core.

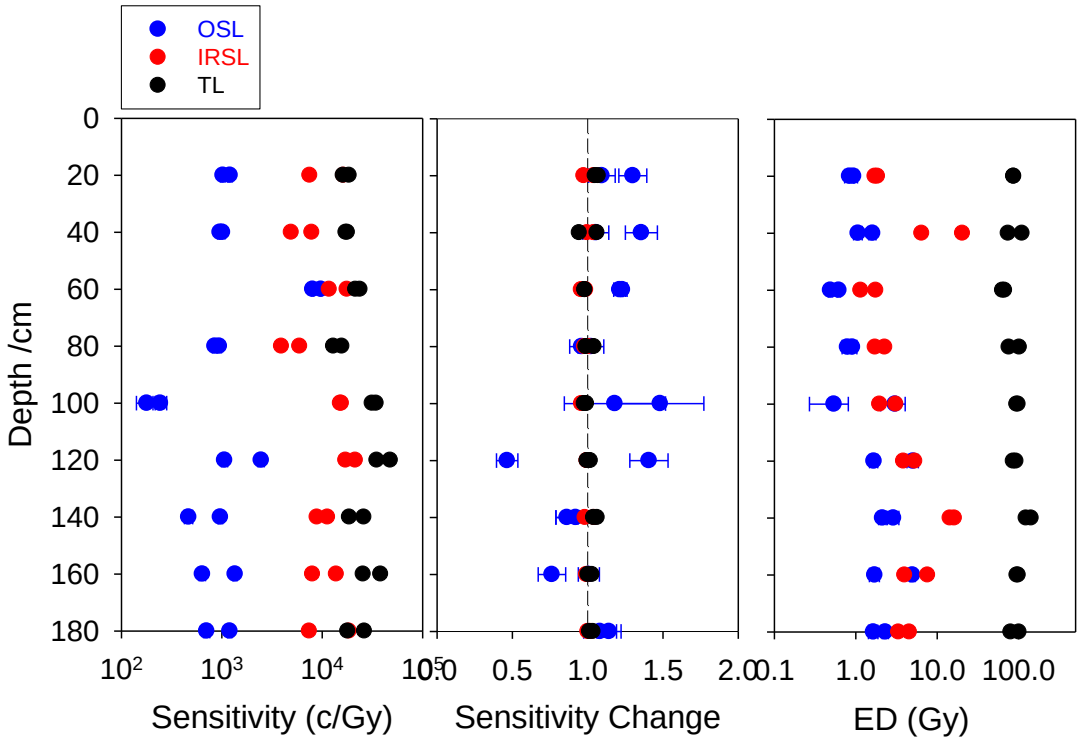

Figure 3.3: Laboratory profiling results for SUTL2959, showing sensitivity for the three measurements (left) the change in sensitivity over the cycle (centre) and estimated stored dose (right).

The laboratory profiling results for SUTL2960 (MON1A) are shown in Fig 3.4, with the sensitivity, sensitivity change and estimated stored dose for the OSL (on the quartz fractions) and IRSL and TL (both on the polymineral fractions). In contrast to SUTL2959, the sensitivities for all three methods are similar, except for the OSL for the first 5 cm which is significantly lower. The sensitivity change for the IRSL and TL is, again, close to unity, with OSL showing a general decrease in sensitivity. The estimated stored dose increases over the first 6 cm, and is subsequently constant down the core. Again, the IRSL estimate is approximately 5x that of the OSL, with the TL estimate being very much higher.

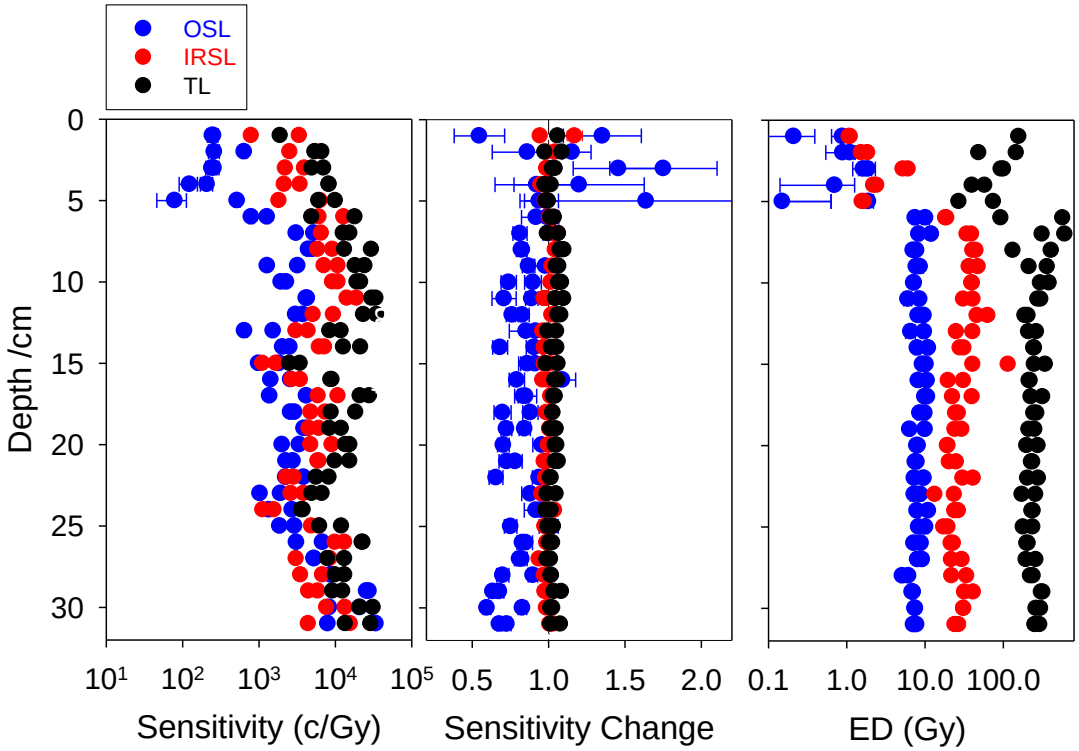

Figure 3.4: Laboratory profiling results for SUTL2960, showing sensitivity for the three measurements (left) the change in sensitivity over the cycle (centre) and estimated stored dose (right).

The laboratory profiling measurements have been conducted using three methods; optically stimulated luminescence (OSL) on 40% HF etched "quartz" mineral grains, infra-red stimulated luminescence (IRSL) and thermoluminescence (TL) on 15% HF etched "polymineral" grains. The OSL measurements, in all cases, show significant sensitivity change over the measurement cycle, and in addition significantly lower signal intensity for the Esmeralda Lake samples (SUTL2959) compared to the other measurements. For Monolith Lake (SUTL2960) all three methods result in comparable signal intensity. For all samples, the stored dose estimates are least for the OSL measurements, increasing for IRSL with TL stored dose estimates very much higher.

The large stored dose estimates from the TL measurements, especially in the top 5 cm of SUTL2960 where stored dose estimates from IRSL and OSL are very much smaller, suggest that charge traps in the 300-500°C range retain inherited geological signals. Similar residual TL signals have been observed from lacustrine sediments from the McMurdo valleys (Doran et.al. 1999), although the residual observed here is significantly larger. Detailed examination of the lower temperature components of the TL glow curves may identify signals that record the dose received since deposition on the lake bed, however this would be a small part of the total signal shown in the profile measurements plotted here. It is therefore concluded that TL may not be the optimal method for quantitative dating analysis of these samples. Previous studies of lacustrine sediments in Antarctica have also shown smaller residual signals for IRSL measurements (Berger & Doran 2001), and the profiling measurements conducted here are also consistent with a small IRSL residual.

The OSL measurements give the lowest stored dose estimates, suggesting that the charge traps in quartz may carry smaller inherited signal than the traps in feldspars within the polymineral samples. The OSL profiling measurements show significant sensitivity changes, and for the Esmeralda (SUTL2959) and in particular the top of the Monolith (SUTL2960) profiles low sensitivity. Nevertheless, the increased likelihood that the quartz grains do not carry inherited signals suggests that these might be the best target for quantitative analysis.

The OSL stored dose estimates for Esmeralda (SUTL2959) show some scatter, but generally follow a slowly increasing trend to greater depth from approximately 0.5 Gy at the top of the profile to approximately 2.0-2.5 Gy at the bottom. There are no obvious step changes in this trend, nor in other measured parameters, that would suggest preferring some of these samples over others for quantitative analysis. In contrast the Monolith profile (SUTL2960) shows a significant increase in stored dose estimates over the first 5 cm of the core, followed by an approximately constant value down the rest of the core. It is suggested that the first 5 cm of the core should be investigated further to quantify this increasing dose region, with one or two additional samples further down the core to confirm the apparent constant age of this section of core.

Samples were thus selected for quantitative analysis, using the SAR OSL procedure on quartz grains, based on the profiling results. All 9 samples from SUTL2959 were carried forward to this analysis. From SUTL2960, 2 samples were selected from the top 5 cm (SUTL2960/2 and SUTL296/5) where profiling indicated an increasing stored dose. Two further samples were selected from the deeper part of the core (SUTL2960/15 and SUTL2960/27) where the profiling indicate an approximately constant stored dose, one from near the middle of this section and one near the bottom, selecting samples where the two profiling aliquots produced similar stored dose variables and where more than 30 g of dried material was available. Dosimetry measurements by beta count rate and HRGS were conducted on all samples that were used for full OSL analysis.

3.3. Laboratory Dosimetry Results

HRGS results are shown in Table 3.1, both as activity concentrations (i.e. disintegrations per second per kilogram) and as equivalent parent element concentrations (in % and ppm), based in the case of U and Th on combining nuclide specific data assuming decay series equilibrium.

Infinite matrix alpha, beta and gamma dose rates from HRGS are listed for all samples in Table 3.2, together with infinite matrix beta dose rates from TSBC.

The water content measurements are given in Table 3.3, together with the assumed values for the average water content during burial. Field (ranging from 3 to 26 % of dry weight) and saturated (18 to 38 % of dry weight) water contents were determined from all samples in the laboratory, with working values for each site adopted for effective dose rate evaluation. Effective dose rates to the HF-etched 150-250 μm quartz grains are given in table 3.3. The effective beta dose rate is a weighted mean of the TSBC and HRGS data, accounting for water content and grain size. The gamma dose rates determined from small samples were relatively poorly defined, but show no

significant variation between neighbouring samples, so to reduce uncertainties the effective mean gamma dose rate is the average of the HRGS data for the sample and the neighbouring samples for SUTL2959 and the average of the top pair and lower pair for SUTL2960, accounting for water content. The total dose rate is the sum of these and the cosmic dose rate.

SUTL no.	Activity Concentration[a] / Bq kg^{-1}			Equivalent Concentration[b]		
	K	U	Th	K / %	U / ppm	Th / ppm
2959/1	724 ± 73	36.6 ± 3.6	49.1 ± 3.1	2.34 ± 0.24	2.97 ± 0.29	12.1 ± 0.8
2959/2	732 ± 71	41.3 ± 3.6	51.4 ± 3.0	2.37 ± 0.23	3.35 ± 0.29	12.7 ± 0.7
2959/3	686 ± 73	30.5 ± 3.6	48.2 ± 2.9	2.22 ± 0.24	2.47 ± 0.29	11.9 ± 0.7
2959/4	775 ± 67	34.4 ± 3.6	51.4 ± 2.9	2.51 ± 0.22	2.79 ± 0.29	12.7 ± 0.7
2959/5	727 ± 85	44.5 ± 5.0	58.8 ± 4.5	2.35 ± 0.27	3.60 ± 0.41	14.5 ± 1.1
2959/6	861 ± 64	45.0 ± 4.2	46.5 ± 3.0	2.78 ± 0.21	3.64 ± 0.34	11.5 ± 0.7
2959/7	718 ± 71	46.3 ± 4.0	50.4 ± 3.1	2.32 ± 0.23	3.75 ± 0.32	12.4 ± 0.8
2959/8	686 ± 83	51.0 ± 5.1	56.7 ± 4.4	2.22 ± 0.27	4.13 ± 0.41	14.0 ± 1.1
2959/9	671 ± 83	49.5 ± 5.2	57.2 ± 4.5	2.17 ± 0.27	4.01 ± 0.42	14.1 ± 1.1
2960/2	536 ± 83	37.8 ± 4.9	42.8 ± 4.3	1.73 ± 0.27	3.07 ± 0.4	10.6 ± 1.1
2960/5	525 ± 70	37 ± 4.2	44.7 ± 3.7	1.7 ± 0.23	3 ± 0.34	11.0 ± 0.9
2960/15	619 ± 66	34.5 ± 3.8	50 ± 2.8	2 ± 0.21	2.79 ± 0.3	12.3 ± 0.7
2960/27	681 ± 65	40.7 ± 3.9	47.1 ± 2.9	2.2 ± 0.21	3.3 ± 0.31	11.6 ± 0.7

Table 3.1: Activity and equivalent concentrations of K, U and Th determined by HRGS

[a]Shap granite reference, working values determined by David Sanderson in 1986, based on HRGS relative to CANMET and NBL standards.

[b]Activity and equivalent concentrations for U, Th and K determined by HRGS (Conversion factors based on NEA (2000) decay constants): 40K: 309.3 Bq kg^{-1} %K^{-1}, 238U: 12.35 Bq kg^{-1} ppmU^{-1}, 232Th: 4.057 Bq kg^{-1} ppm Th^{-1}

SUTL no.	HRGS, dry[a] / mGy a^{-1}			TSBC, dry / mGy a^{-1}
	Alpha	Beta	Gamma	
2959/1	17.19 ± 0.99	2.72 ± 0.20	1.53 ± 0.08	3.21 ± 0.10
2959/2	18.67 ± 0.97	2.82 ± 0.20	1.61 ± 0.07	2.96 ± 0.10
2959/3	15.64 ± 0.98	2.54 ± 0.20	1.43 ± 0.08	2.78 ± 0.09
2959/4	17.10 ± 0.97	2.85 ± 0.19	1.57 ± 0.07	2.41 ± 0.09
2959/5	20.74 ± 1.39	2.89 ± 0.24	1.73 ± 0.10	2.92 ± 0.11
2959/6	18.60 ± 1.10	3.17 ± 0.18	1.68 ± 0.07	2.78 ± 0.09
2959/7	19.61 ± 1.06	2.83 ± 0.20	1.63 ± 0.08	2.80 ± 0.09
2959/8	21.81 ± 1.40	2.84 ± 0.23	1.73 ± 0.10	2.88 ± 0.11
2959/9	21.55 ± 1.43	2.79 ± 0.23	1.71 ± 0.10	2.86 ± 0.11
2960/2	16.32 ± 1.36	2.19 ± 0.23	1.31 ± 0.10	1.98 ± 0.07
2960/5	16.47 ± 1.16	2.16 ± 0.20	1.32 ± 0.08	2.13 ± 0.08
2960/15	16.87 ± 0.99	2.42 ± 0.18	1.44 ± 0.07	2.72 ± 0.07
2960/27	17.75 ± 1.01	2.64 ± 0.18	1.51 ± 0.07	2.67 ± 0.07

Table 3.2: Infinite matrix dose rates determined by HRGS and TSBC

[a]based on dose rate conversion factors in Aikten (1983) and Sanderson (1987)

SUTL no.	Water contents / %			Effective Dose Rate / mGy a^{-1}		
	Field	Parallel[a]	Assumed	Beta[b]	Gamma[c]	Total[d]
2959/1	4.7	16.7	20 ± 5	2.24 ± 0.13	1.28 ± 0.07	3.71 ± 0.15
2959/2	8.1	20.5	20 ± 5	2.11 ± 0.12	1.25 ± 0.07	3.53 ± 0.14
2959/3	13.6	20.6	20 ± 5	1.98 ± 0.12	1.26 ± 0.07	3.40 ± 0.13
2959/4	17.7	21.1	20 ± 5	1.80 ± 0.11	1.29 ± 0.07	3.26 ± 0.13
2959/5	18.8	24.8	20 ± 5	2.09 ± 0.13	1.36 ± 0.07	3.62 ± 0.15
2959/6	11.1	22.5	20 ± 5	2.07 ± 0.12	1.37 ± 0.07	3.60 ± 0.14
2959/7	3.6	25.6	20 ± 5	2.02 ± 0.12	1.37 ± 0.07	3.55 ± 0.14
2959/8	7.5	25.3	20 ± 5	2.06 ± 0.13	1.38 ± 0.08	3.60 ± 0.15
2959/9	9.9	30.9	20 ± 5	2.04 ± 0.12	1.41 ± 0.07	3.60 ± 0.15
	Field	Sat	Assumed			
2960/2	45.4	60.5	50 ± 5	1.10 ± 0.06	0.85 ± 0.04	2.12 ± 0.07
2960/5	41.5	53.3	50 ± 5	1.18 ± 0.06	0.85 ± 0.04	2.19 ± 0.08
2960/15	17.7	23.9	20 ± 5	1.93 ± 0.11	1.20 ± 0.06	3.30 ± 0.13
2960/27	14.7	26.9	20 ± 5	1.92 ± 0.11	1.20 ± 0.06	3.29 ± 0.12

Table 3.3: Effective beta and gamma dose rates following water correction.

[a] For SUTL2959 the samples may have partially dried prior to water content measurement and saturated water content was not measured, additional water contents for a parallel core (ESM3/14) are available and tabulated.
[b] Effective beta dose rate combining water content corrections with inverse grain size attenuation factors obtained by weighting the 150-250 μm attenuation factors of Mejdahl (1979) for K, U, and Th by the relative beta dose contributions for each source determined by Gamma Spectrometry;
[c] Mean of sample and neighbouring samples from HRGS with water content corrections
[d] includes a cosmic dose contribution

3.4. Quartz single aliquot equivalent dose determinations

For equivalent dose determination, data from single aliquot regenerative dose measurements were analysed using the Risø TL/OSL Viewer programme to export integrated summary files that were analysed in MS Excel and SigmaPlot. Composite dose response curves were constructed from selected discs and when possible, for each of the preheating groups from each sample, and used to estimate equivalent dose values for each individual disc and their combined sets. Dose response curves (shown in Appendix C) for each of the preheating temperature groups and the combined data sets. Routinely these curves would be determined using a fit to a saturating exponential function passing through the origin. It's noted that the data show a significant zero dose signal, and a linear fit for each individual aliquot conducted. Probability density functions (PDFs) and abanico plots were generated to describe the dose distributions, and are shown in Appendix D.

SAR quality parameters are given in Table 3.4. Most of these samples are relatively low sensitivity, with less than 3000 c Gy^{-1}, with SUTL2960/2 and 2960/5 showing lower sensitivity as expected from the profile measurements. The samples all show a slight decrease in sensitivity of 5-10% per cycle. In most cases, they demonstrate negligible IRSL signals, with the exception being SUTL2960/15 which also showed a considerable slow OSL component that built up during the measurement cycle. Recycling ratios should be unity, and range from 0.91 to 1.11 with an average of 0.98 ± 0.02. It is noted that SUTL2960/15 has a recycling ratio of 0.91 ± 0.03, significantly below unity. In all cases the zero cycle measurement is significantly greater than zero. A dose recovery test is conducted using the first test dose normalised using the subsequent regenerative dose (equal to the test dose) as an N/TD value to calculate the equivalent dose, the values tabulated in Table 3.4 is the weighted mean and standard

error on ratio of the calculated recovered dose to the applied dose, and with the exception of SUTL2960/15 (with a ratio of 1.64 ± 0.05), are within measurement uncertainties of unity.

SUTL no.	Mean sensitivity c Gy^{-1}	Sensitivity change / cycle (%)	Recycling ratio	Zero cycle	IRSL (%)	Dose recovery
2959/1	1136 ± 138	-6.4 ± 2.9	0.978 ± 0.081	0.82 ± 0.07	-1.7 ± 1.8	1.11 ± 0.17
2959/2	1624 ± 358	-7.7 ± 3.7	0.924 ± 0.066	0.77 ± 0.06	1.0 ± 2.0	0.80 ± 0.16
2959/3	1982 ± 205	-7.2 ± 2.4	0.975 ± 0.049	0.84 ± 0.09	-2.8 ± 1.4	1.16 ± 0.11
2959/4	1860 ± 216	-7.5 ± 2.7	0.989 ± 0.043	0.90 ± 0.04	1.5 ± 1.2	0.84 ± 0.11
2959/5	1883 ± 139	-7.2 ± 1.7	0.946 ± 0.033	0.93 ± 0.05	1.5 ± 0.9	0.91 ± 0.14
2959/6	3879 ± 395	-7.6 ± 2.4	0.934 ± 0.027	0.83 ± 0.04	0.0 ± 0.6	1.14 ± 0.10
2959/7	2866 ± 258	-7.9 ± 2.1	0.923 ± 0.030	0.86 ± 0.03	1.1 ± 0.5	1.06 ± 0.10
2959/8	2277 ± 170	-8.0 ± 1.7	0.972 ± 0.036	0.88 ± 0.05	-0.8 ± 0.7	1.05 ± 0.13
2959/9	3107 ± 281	-7.6 ± 2.1	1.003 ± 0.034	0.88 ± 0.03	0.9 ± 0.6	1.01 ± 0.09
2960/2	659 ± 79	-5.1 ± 2.8	1.068 ± 0.077	0.58 ± 0.10	4.1 ± 3.4	1.07 ± 0.23
2960/5	1013 ± 113	-7.7 ± 2.6	1.114 ± 0.079	0.87 ± 0.05	-0.7 ± 2.0	1.13 ± 0.29
2960/15	9482 ± 1292	-11.0 ± 3.0	0.907 ± 0.034	0.35 ± 0.06	48.8 ± 1.3	1.64 ± 0.05
2960/27	2835 ± 256	-8.1 ± 2.1	0.979 ± 0.034	0.85 ± 0.05	0.0 ± 0.9	1.02 ± 0.11

Table 3.4: SAR quality parameters

For each sample, the mean, weighted mean and a robust mean were calculated, as given in Table 3.5. The dose distributions for each sample (Appendix D) all show a broad range of doses, in many cases with multiple peaks or shoulders, and tails to higher dose. The mean estimate that most closely matches the centre of the major peak has generally been selected, where there are multiple peaks the lower peak is chosen as mostly likely representing the minimum age. The chosen mean is indicated in bold type in Table 3.5, and shown on the plots in Appendix D.

The calculated ages for these samples are given in Table 3.6, combined the preferred stored dose estimate (Table 3.5) with the total dose rate (Table 3.3). These ages are plotted as a function of depth (Fig. 3.5), along with apparent ages from the profiling results determined from the stored dose estimates (Figs 3.3 and 3.4, Tables B.1 and B.2) combined with dose rates determined for the OSL samples (Table 3.3), interpolated for the SUTL2960 profiling samples not carried forward for OSL SAR. The data for these plots is tabulated in Appendix E.

SUTL no.	Comments on stored dose distribution / individual samples	Mean	Weighted Mean	Robust Mean	Profile OSL
2959/1	Broad peak with maximum at ~1.0 Gy, second peak at ~3.0 Gy, with tail to ~8 Gy	1.65 ± 0.36	**0.97 ± 0.17**	1.57 ± 0.11	0.89 ± 0.11
2959/2	Broad peak with maximum at ~0.5-2.0 Gy, with tail to ~8 Gy	1.21 ± 0.26	0.84 ± 0.17	**1.11 ± 0.25**	1.34 ± 0.15
2959/3	Double peak with maxima at ~0.5 Gy and ~1.5 Gy, tail to 5 Gy	0.86 ± 0.25	**0.42 ± 0.10**	0.90 ± 0.09	0.56 ± 0.03
2959/4	Multiple peaks at ~0.2, 1.0, 2.0 and 3.0 Gy, tail to 6 Gy	1.28 ± 0.28	**1.14 ± 0.12**	1.28 ± 0.43	0.85 ± 0.11
2959/5	Broad peak with maximum at ~1.2 Gy, with tail to ~5 Gy	1.16 ± 0.17	0.98 ± 0.15	**1.17 ± 0.09**	1.79 ± 0.74
2959/6	Narrow peak with maximum at ~1.3 Gy, with second broad peak ~3-5 Gy, tail to ~8 Gy Includes one aliquot 23 ± 3 Gy	3.67 ± 1.47	**1.31 ± 0.11**	2.38 ± 0.57	3.37 ± 0.59
2959/7	Four distinct peaks at ~1.5, 5.0, 7.0 and 12.0 Gy	4.70 ± 0.90	2.83 ± 0.16	4.18 ± 0.13	2.52 ± 0.37
	mean of data contributing to ~1.5 Gy peak	1.91 ± 0.22	**1.70 ± 0.67**	1.91 ± 0.06	
2959/8	Two broad peaks with maxima at ~0.5-1.5 and ~3.0 Gy, tail to 7 Gy	3.17 ± 1.29	**1.17 ± 0.15**	1.84 ± 0.52	3.34 ± 0.32
2959/9	Broad peak with maximum at ~2.0-3.0 Gy, with tail to ~10 Gy	2.52 ± 0.53	**1.32 ± 0.10**	2.41 ± 0.61	1.98 ± 0.21
2960/2	Broad peak ~0-2.0 Gy, tail to ~8 Gy.	**1.01 ± 0.35**	0.82 ± 0.25	1.10 ± 0.09	0.99 ± 0.19
2960/5	Peak at ~1.0-1.5 Gy, shoulder at ~3 Gy, tail to ~10 Gy	2.39 ± 0.73	**0.88 ± 0.25**	1.70 ± 0.51	1.02 ± 0.28
2960/15	Four distinct peaks at ~3, 6, 8 and 11 Gy. Note: values based on data with large IRSL, and that fail recycling and dose recovery tests	7.57 ± 0.47	6.36 ± 0.11	**7.60 ± 0.05**	9.78 ± 0.63
2960/27	Broad peak with maximum at ~3.0-6.0 Gy, with tail to>20 Gy. Three saturated aliquots removed from analysis	9.75 ± 0.68	**8.03 ± 0.38**	9.43 ± 0.73	8.64 ± 0.27

Table 3.5: Comments on equivalent dose distributions; preferred estimates in bold

errors stated: ± weighted standard deviation (weighted error)

SUTL no.	Dose (Gy)	Dose Rate (mGy a^{-1})	Years / ka	Calendar years
2959/1	0.97 ± 0.17	3.71 ± 0.15	0.26 ± 0.05	1756 ± 47 AD
2959/2	1.11 ± 0.25	3.53 ± 0.14	0.31 ± 0.07	1703 ± 72 AD
2959/3	0.42 ± 0.10	3.40 ± 0.13	0.12 ± 0.03	1893 ± 30 AD
2959/4	1.14 ± 0.12	3.26 ± 0.13	0.35 ± 0.04	1667 ± 39 AD
2959/5	1.17 ± 0.09	3.62 ± 0.15	0.32 ± 0.03	1694 ± 28 AD
2959/6	1.31 ± 0.11	3.60 ± 0.14	0.36 ± 0.03	1653 ± 34 AD
2959/7	1.70 ± 0.67	3.55 ± 0.14	0.48 ± 0.19	1538 ± 190 AD
2959/8	1.17 ± 0.15	3.60 ± 0.15	0.33 ± 0.04	1692 ± 44 AD
2959/9	1.32 ± 0.10	3.60 ± 0.15	0.37 ± 0.03	1650 ± 32 AD
2960/2	1.01 ± 0.35	2.12 ± 0.07	0.48 ± 0.17	1541 ± 166 AD
2960/5	0.88 ± 0.25	2.19 ± 0.08	0.40 ± 0.12	1615 ± 115 AD
2960/15†	7.60 ± 0.05	3.30 ± 0.13	2.30 ± 0.09	286 ± 92 BC
2960/27	8.03 ± 0.38	3.29 ± 0.12	2.44 ± 0.15	424 ± 146 BC

Table 3.6: Quartz OSL ages

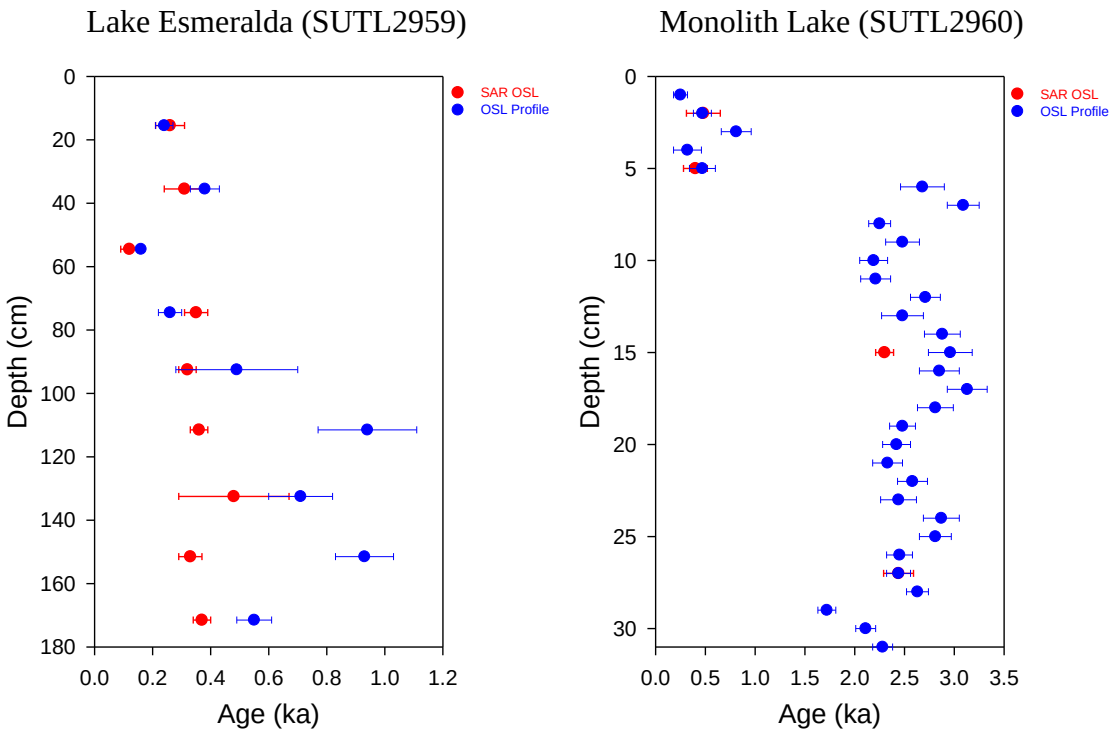

Figure 3.5: Age depth profiles for the Lake Esmeralda core (SUTL2959, ESM-3) and Monolith Lake core (SUTL2960, MON-1A). Showing ages determined from SAR OSL measurements (red) and apparent ages from the profile measurements (blue).

3.5. Scanning Electron Microscopy

Optical and Scanning Electron Microscopy (SEM) was used to characterise the mineral grains on selected samples, in particular to assess the quality of mineral extraction and to determine if non-quartz minerals or inclusions could explain the different luminescence behaviour of SUTL2960/15 compared to the other samples.

Two or three discs from samples SUTL2960/5, 2960/15 and 2960/27 were examined under an optical microscope. In all cases this showed clean grains of approximately uniform size, with approximately 50% white and milky in appearance and 50% clear. A small number of grains included dark bands and spots. For SUTL2960/15 one aliquot contained a single black grain in the region examined, and another aliquot a single pink grain. No coloured grains were observed in any of the aliquots of the other two samples.

Small areas of single aliquots for each of these samples were examined under the SEM to identify elemental compositions of spots on individual grains. Examples of x-ray spectra recorded from these samples are shown in Figure 3.6. Again, all three samples were very similar with the majority of grains composed of Si and O without other elements measured. A small number of grains included areas with different a appearance under the SEM, and examination of these showed that some of these areas contained Al with K or Ca (feldspars), other areas were enriched with Fe and Ti. The number of these inclusions is very small, but they may be slightly more numerous on the disc for SUTL2960/15.

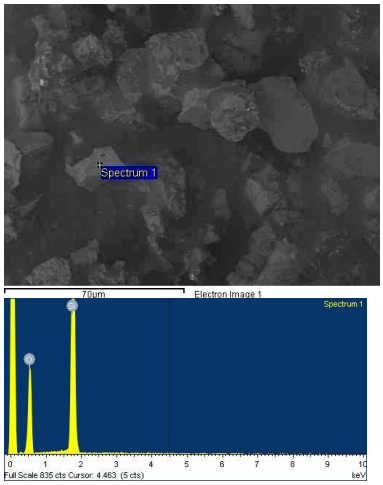

SUTL2690/5 Example spectrum from smooth surfaced grains. Other similar appearing grains show the same Si & O composition.

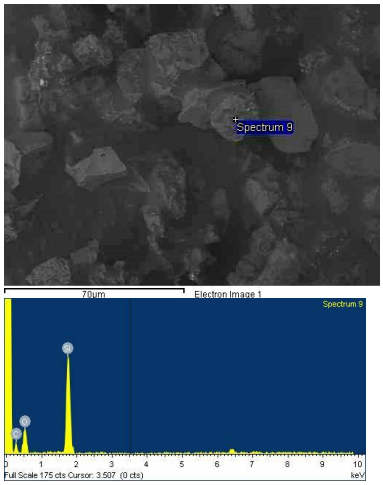

SUTL2690/5 Example spectrum from rougher surfaced grains. Other similar appearing grains show the same Si & O composition.

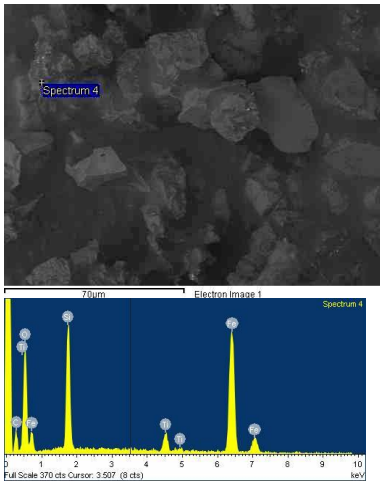

SUTL2690/5 Example spectrum from bright inclusion showing Fe & Ti x-rays. Other bright inclusions are similar, or just Si & O.

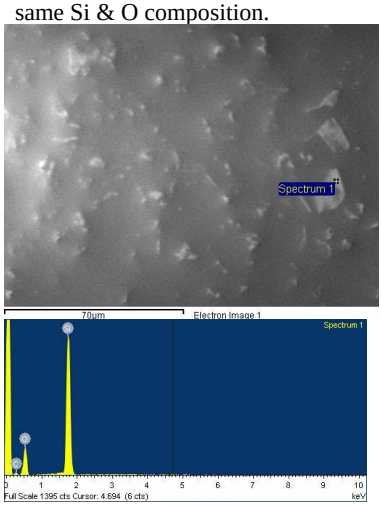

SUTL2690/15 Example spectrum from smooth surfaced grains. Other similar appearing grains show the same Si & O composition.

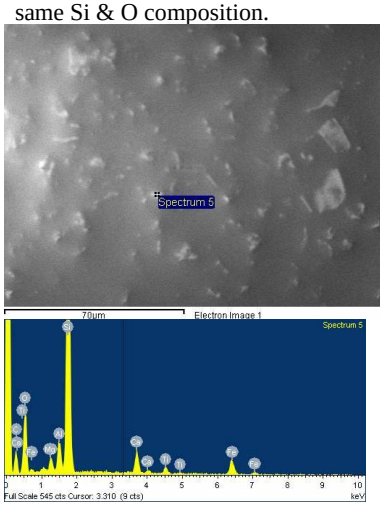

SUTL2690/15 Example spectrum from bright inclusion showing Fe & Ti x-rays, with Al & Ca suggesting feldspar. Other bright inclusions on this scene contain Si & O only.

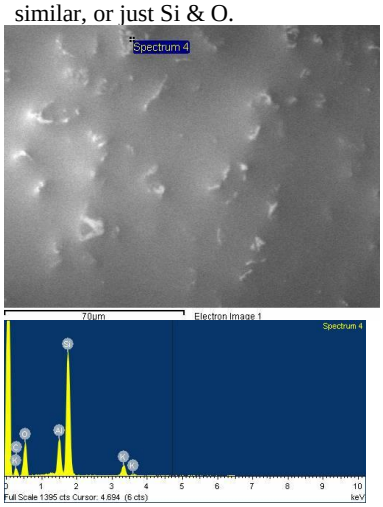

SUTL2690/15 Example spectrum from rougher appearing grain showing Al & K suggesting feldspar. Other grains on this scene contain Si & O only.

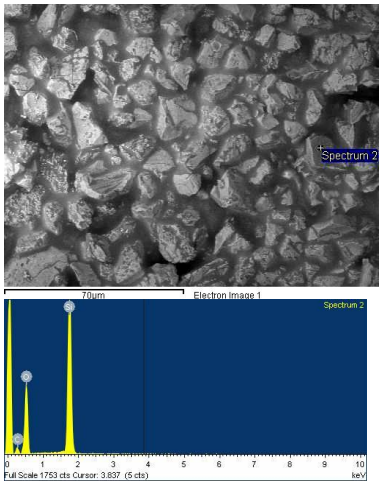

SUTL2690/27 Example spectrum from smooth surfaced grains. Other similar appearing grains show the same Si & O composition.

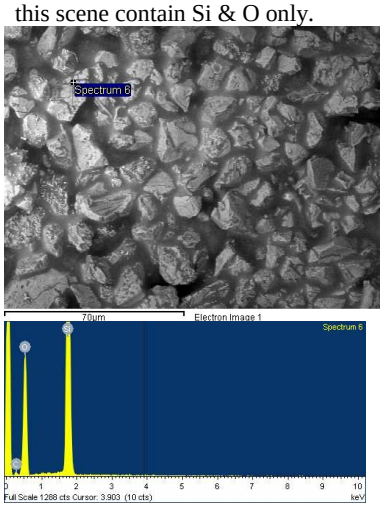

SUTL2690/27 Example spectrum from rougher surfaced grains. Most other similar appearing grains show the same Si & O composition.

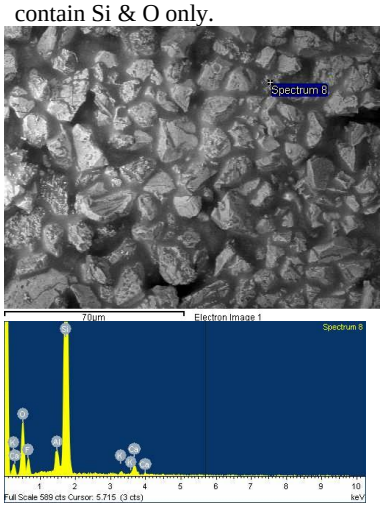

SUTL2690/27 Spectrum from a rougher surfaced grain showing Al, K and Ca, suggesting a feldspar grain or inclusion.

Figure 3.6: Example SEM spectra from SUTL2960/5, 2960/15 and 2960/27.

4. Discussion and conclusions

Luminescence profiling has been conducted on two cores from lakes on the James Ross Island archipelago, Lake Esmeralda and Monolith Lake. Measurements on bulk sediments using the SUERC Portable OSL instrument showed no trend in either the IRSL or OSL signals for the Lake Esmeralda samples (SUTL2959), whereas for the Monolith Lake samples (SUTL2960) both the IRSL and OSL signals increase over the first 10 cm before forming a plateau with a further gradual increase from about 25 cm down the core. The laboratory profile measurements show a significant difference in sensitivity for the three readout methods used, with OSL on the nominal quartz fraction showing the lowest sensitivity followed by IRSL and then TL on the poly-mineral fraction. The OSL showed some sensitivity changes, whereas the IRSL and TL did not. There was also a significant difference in estimated stored dose, with the OSL giving the lowest doses (0.5 - 3.4 Gy for SUTL2959, 0.5 - 10.3 Gy for SUTL2960), followed by IRSL (1.5 - 17.0 Gy for SUTL2959, 1.1 - 54.9 Gy for SUTL2960) with TL giving doses of >100 Gy for all samples. The OSL profile measurements for SUTL2959 show a trend to slowly increasing estimated dose with depth, whereas for SUTL2960 the top 5 samples give low estimated stored doses (~0.5 - 1.0 Gy) with a substantial step to higher doses (~8 - 10 Gy) for the lower part of the core.

Based on the profiling measurements it was decided to pursue OSL measurements on quartz for quantitative analysis of all nine samples from Lake Esmeralda and four samples selected from the Monolith Lake core - two from the low dose, low sensitivity section (SUTL2960/2 and 2960/5), and two from the higher dose, higher sensitivity section (SUTL2960/15 and 2960/27). Dose rates were determined for all these samples using thick source beta counting (TSBC) and high resolution gamma spectrometry (HRGS), with the total dose rate determined from a combination of these measurements and a calculated cosmic dose rate. The samples were processed to extract 150-250 µm quartz grains, which were dispensed to 16 stainless steel discs. These were analysed using a single aliquot regenerative (SAR) approach to determine the stored dose for each aliquot, with the weighted mean of all the aliquots that satisfied SAR quality checks combined with the dose rate used to determine the age of each sample.

The apparent ages from the OSL estimated dose from the profile measurements combined with interpolated dose rates are very similar to the corresponding quantitative SAR analysis ages. For Lake Esmeralda, the ages show a general increase with depth, from 0.4 to 0.8 ka, with some minor steps down in age between 40 and 50 cm and between 140 and 150 cm. For Monolith Lake, the ages show a young component at ~0.5 ka over the top 5 cm, then a step to 2.5-3.0 ka with cyclical variations over ~0.5 ka for most of the core. Below 26 cm, the final three profile apparent ages are significantly lower in age and form a progression of older aged material at greater depth.

The entirety of the Lake Esmeralda core fits within the time scale for the top 5 cm of the Monolith Lake core. The top of the Monolith Lake core shows significant differences from the lower section, in particular significantly lower luminescence sensitivity and much younger OSL ages. Within the last 1000 years there has been a significant change in the sediment supply to Monolith Lake. The age profile for

Monolith Lake, in particular the younger ages for material below 26 cm, suggests that the sediments below 5 cm carried a residual dose when they were deposited in the lake, with the deepest sediments in the core carrying a smaller residual or being reset and thus giving a true age for these layers. The larger doses measured by IRSL and TL in the profiling indicate that it is likely that the luminescence centres associated with these signals carried a residual dose for all samples. Further exploration of these signals may reveal additional information on the sediment histories.

5. References

Aitken, M.J., 1983, Dose rate data in SI units: PACT, v. 9, p. 69–76.

Berger, G.W., Doran, P.T., 2001, Luminescence-dating zeroing tests in Lake Hoare, Taylor Valley, Antarctica. Journal of Paleolimnology, v. 25, pp. 519-529.

Björck et al 1996 ???

Doran, P.T., Berger, G.W., Lyons, W.B., Wharton, R.A., Davisson, M.L., Southon, J., Dibb, J.E., 1999, Dating Quaternary lacustrine sediments in the McMurdo Dry Valleys, Antarctica. Paleogeography, Paleoclimatology, Paleoecology, v. 147, pp. 223-239.

Hodgson, D.A., Roberts, S.J., Bentley, M.J., Smith, J.A., Johnson, J.S., Verleyen, E., Vyverman, W., Hodson, A.J., Leng, M.J., Cziferszky, A., Fox, A.J., Sanderson, D.C.W., 2009a, Exploring former subglacial Hodgson Lake, Antarctica Paper I: site description, geomorphology and limnology. Quaternary Science Reviews, v. 28, pp. 2295-2309.

Hodgson, D.A., Roberts, S.J., Bentley, M.J., Carmichael, E.L., Smith, J.A., Verleyen, E., Vyverman, W., Geissler, P., Leng, M.J., Sanderson, D.C.W., 2009b, Exploring former subglacial Hodgson Lake, Antarctica Paper II: paleolimnology. Quaternary Science Reviews, v. 28, pp. 2310-2325.

Krause, W.E., Krbetschek, M.R., Stolz, W., 1997, Dating of quaternary lake sediments from the Schirmacher Oasis (East Antarctica) by infra-red stimulated luminescence (IRSL) detected at the wavelength of 560 nm. Quaternary Science Reviews, v. 16, pp. 387-392.

Mejdahl, V., 1979, Thermoluminescence dating: Beta-dose attenuation in quartz grains Archaeometry, v. 21, p. 61-72.

Mejdahl, V., 1983, Feldspar inclusion dating of ceramics and burnt stones, PACT, v. 9, p. 351-364.

NEA, 2000, The JEF-2.2 Nuclear Data Library: Nuclear Energy Agency, Organisation for economic Co-operation and Development. JEFF Report, v. 17.

Prescott, J.R., and Hutton, J.T., 1994, Cosmic ray contributions to dose rates for luminescence and ESR dating: Large depths and long-term time variations: Radiation Measurements, v. 23, p. 497-500.

Roberts, S.J., Hodgson, D.A., Bentley, M.J., Sanderson, D.C.W., Milne, G., Smith, J.A., Verleyen, E., Balbo, A., 2009, Holocene relative sea-level change and deglaciation on Alexander Island, Antarctic Peninsula, from elevated lake deltas. Geomorphology, v. 112, pp. 122-134.

Sanderson, D.C.W., 1987, Thermoluminescence dating of vitrified Scottish Forts: Paisley, Paisley college.

—, 1988, Thick source beta counting (TSBC): A rapid method for measuring beta dose-rates: International Journal of Radiation Applications and Instrumentation. Part D. Nuclear Tracks and Radiation Measurements, v. 14, p. 203-207.

Appendix A: Water content measurements

Sample	Water Content (%)		
	Wet	Saturated	Assumed
SUTL2960/1	45.4	46.4	45 ± 5
SUTL2960/2	45.4	60.5	50 ± 5
SUTL2960/3	43.6	56.5	50 ± 5
SUTL2960/4	43.8	54.2	50 ± 5
SUTL2960/5	41.5	53.3	50 ± 5
SUTL2960/6	39.2	53.2	50 ± 5
SUTL2960/7	27.2	40.3	35 ±5
SUTL2960/8	20.7	33.4	25 ± 5
SUTL2960/9	18.4	29.2	20 ± 5
SUTL2960/10	17.8	25.6	20 ± 5
SUTL2960/11	14.0	24.5	20 ± 5
SUTL2960/12	17.9	28.2	20 ± 5
SUTL2960/13	16.9	24.5	20 ± 5
SUTL2960/14	17.5	27.9	20 ± 5
SUTL2960/15	17.7	23.9	20 ± 5
SUTL2960/16	17.8	27.3	20 ± 5
SUTL2960/17	17.1	26.5	20 ± 5
SUTL2960/18	17.0	22.9	20 ± 5
SUTL2960/19	17.3	24.7	20 ± 5
SUTL2960/20	17.7	26.5	20 ± 5
SUTL2960/21	17.9	29.2	20 ± 5
SUTL2960/22	17.6	24.3	20 ± 5
SUTL2960/23	18.0	24.4	20 ± 5
SUTL2960/24	16.0	24.9	20 ± 5
SUTL2960/25	16.1	23.9	20 ± 5
SUTL2960/26	15.8	26.7	20 ± 5
SUTL2960/27	14.7	26.9	20 ± 5
SUTL2960/28	15.5	28.7	20 ± 5
SUTL2960/29	15.0	27.5	20 ± 5
SUTL2960/30	14.7	26.2	20 ± 5
SUTL2960/31	15.0	24.5	20 ± 5

Table A.1: Measured water contents for the Monolith Lake core (SUTL2960) sections as received (wet) and saturated, with assumed average water content during burial.

Appendix B: Profiling Results

Table B.1: Instrumental profiling results for Lake Esmeralda (SUTL2959)

SUTL No.	Aliquot	IRSL		OSL		IRSL : OSL
		Net Counts	Depletion	Net Counts	Depletion	
2959/1	1	118090 ± 349	1.363 ± 0.008	722226 ± 855	1.300 ± 0.003	0.1635 ± 0.0005
	2	65693 ± 262	1.341 ± 0.011	656863 ± 815	1.234 ± 0.003	0.1000 ± 0.0004
	Mean	91892 ± 218	1.352 ± 0.007	689545 ± 590	1.267 ± 0.002	0.1318 ± 0.0003
2959/2	1	10450 ± 113	1.351 ± 0.028	186988 ± 436	1.064 ± 0.005	0.0559 ± 0.0006
	2	13121 ± 127	1.304 ± 0.024	295849 ± 549	1.069 ± 0.004	0.0444 ± 0.0004
	Mean	11786 ± 85	1.328 ± 0.018	241419 ± 351	1.066 ± 0.003	0.0501 ± 0.0004
2959/3	1	43032 ± 214	1.328 ± 0.013	405116 ± 640	1.122 ± 0.004	0.1062 ± 0.0006
	2	34364 ± 194	1.324 ± 0.015	315458 ± 566	1.147 ± 0.004	0.1089 ± 0.0006
	Mean	38698 ± 144	1.326 ± 0.010	360287 ± 427	1.135 ± 0.003	0.1076 ± 0.0004
2959/4	1	2892 ± 73	1.402 ± 0.059	47654 ± 225	1.055 ± 0.010	0.0607 ± 0.0016
	2	5781 ± 94	1.311 ± 0.037	63751 ± 259	1.107 ± 0.009	0.0907 ± 0.0015
	Mean	4337 ± 60	1.356 ± 0.035	55703 ± 172	1.081 ± 0.007	0.0757 ± 0.0011
2959/5	1	25705 ± 166	1.370 ± 0.018	439143 ± 666	1.121 ± 0.003	0.0585 ± 0.0004
	2	23107 ± 160	1.303 ± 0.018	430205 ± 659	1.084 ± 0.003	0.0537 ± 0.0004
	Mean	24406 ± 115	1.337 ± 0.012	434674 ± 469	1.103 ± 0.002	0.0561 ± 0.0003
2959/6	1	53308 ± 238	1.302 ± 0.012	660665 ± 817	1.261 ± 0.003	0.0807 ± 0.0004
	2	68229 ± 268	1.349 ± 0.011	626196 ± 796	1.185 ± 0.003	0.1090 ± 0.0004
	Mean	60769 ± 179	1.326 ± 0.008	643431 ± 570	1.223 ± 0.002	0.0948 ± 0.0003
2959/7	1	68487 ± 269	1.361 ± 0.011	405489 ± 641	1.109 ± 0.003	0.1689 ± 0.0007
	2	93563 ± 311	1.370 ± 0.009	456482 ± 681	1.266 ± 0.004	0.2050 ± 0.0007
	Mean	81025 ± 206	1.366 ± 0.007	430986 ± 468	1.187 ± 0.003	0.1869 ± 0.0005
2959/8	1	22017 ± 159	1.328 ± 0.018	257500 ± 513	1.177 ± 0.005	0.0855 ± 0.0006
	2	15426 ± 135	1.413 ± 0.024	174521 ± 423	1.151 ± 0.006	0.0884 ± 0.0008
	Mean	18722 ± 104	1.370 ± 0.015	216011 ± 332	1.164 ± 0.004	0.0869 ± 0.0005
2959/9	1	9801 ± 113	1.267 ± 0.027	150478 ± 393	1.120 ± 0.006	0.0651 ± 0.0008
	2	11143 ± 118	1.288 ± 0.026	172326 ± 420	1.109 ± 0.005	0.0647 ± 0.0007
	Mean	10472 ± 82	1.277 ± 0.019	161402 ± 288	1.115 ± 0.004	0.0649 ± 0.0005

Table B.2: Laboratory profiling results for Lake Esmeralda (SUTL2959)

SUTL No.	Aliquot	Quartz (OSL)			Polymineral (IRSL)			Polymineral (TL)		
		Sensitivity (c Gy^{-1})	Sensitivity change	Ed (Gy)	Sensitivity (c Gy^{-1})	Sensitivity change	Ed (Gy)	Sensitivity (c Gy^{-1})	Sensitivity change	Ed (Gy)
2959/1	1	1208 ± 65	1.300 ± 0.093	0.94 ± 0.11	16337 ± 77	0.975 ± 0.007	1.72 ± 0.02	18559 ± 62	1.050 ± 0.005	87.13 ± 0.30
	2	1027 ± 59	1.095 ± 0.088	0.84 ± 0.11	7526 ± 54	1.04 ± 0.011	1.85 ± 0.03	16156 ± 57	1.071 ± 0.005	86.68 ± 0.32
	Mean	1117 ± 62	1.20 ± 0.09	0.89 ± 0.11	11932 ± 47	1.01 ± 0.01	1.79 ± 0.03	17358 ± 42	1.06 ± 0.01	86.9 ± 0.22
2959/2	1	1014 ± 62	1.357 ± 0.106	1.61 ± 0.16	4910 ± 45	0.997 ± 0.013	6.45 ± 0.08	17813 ± 60	0.945 ± 0.004	74.47 ± 0.26
	2	961 ± 55	1.054 ± 0.086	1.07 ± 0.13	7867 ± 55	1.04 ± 0.011	20.43 ± 0.16	17211 ± 59	1.062 ± 0.005	110.44 ± 0.39
	Mean	988 ± 59	1.21 ± 0.10	1.34 ± 0.15	6389 ± 36	1.02 ± 0.01	13.4 ± 3.5	17512 ± 42	1.00 ± 0.01	92.45 ± 0.23
2959/3	1	9723 ± 181	1.231 ± 0.031	0.62 ± 0.03	11757 ± 65	0.987 ± 0.008	1.76 ± 0.02	23751 ± 70	0.981 ± 0.004	67.38 ± 0.20
	2	8039 ± 194	1.213 ± 0.040	0.49 ± 0.03	17663 ± 79	0.958 ± 0.006	1.15 ± 0.01	21507 ± 66	0.981 ± 0.004	63.32 ± 0.20
	Mean	8881 ± 188	1.22 ± 0.04	0.56 ± 0.03	14710 ± 51	0.97 ± 0.01	1.45 ± 0.02	22629 ± 48	0.98 ± 0.01	65.35 ± 0.14
2959/4	1	854 ± 49	1.022 ± 0.085	0.79 ± 0.11	5967 ± 47	0.979 ± 0.011	2.27 ± 0.04	15698 ± 57	0.988 ± 0.005	76.23 ± 0.28
	2	941 ± 51	0.960 ± 0.079	0.91 ± 0.12	3926 ± 40	1.006 ± 0.014	1.73 ± 0.04	12948 ± 51	1.042 ± 0.006	102.16 ± 0.42
	Mean	897 ± 50	0.99 ± 0.08	0.85 ± 0.11	4946 ± 31	0.99 ± 0.01	2.00 ± 0.04	14323 ± 38	1.02 ± 0.01	89.19 ± 0.25
2959/5	1	244 ± 38	1.482 ± 0.290	0.54 ± 0.27	15137 ± 75	0.959 ± 0.007	3.10 ± 0.03	34447 ± 84	0.993 ± 0.003	94.83 ± 0.24
	2	179 ± 38	1.181 ± 0.336	3.04 ± 1.01	15527 ± 75	0.97 ± 0.007	1.96 ± 0.02	31410 ± 80	0.978 ± 0.004	98.47 ± 0.26
	Mean	211 ± 38	1.33 ± 0.31	1.79 ± 0.74	15332 ± 53	0.96 ± 0.01	2.53 ± 0.03	32928 ± 58	0.99 ± 0.01	96.65 ± 0.17
2959/6	1	1065 ± 75	1.407 ± 0.127	1.67 ± 0.19	21404 ± 90	0.997 ± 0.006	3.86 ± 0.03	47666 ± 99	0.995 ± 0.003	85.88 ± 0.18
	2	2466 ± 174	0.466 ± 0.071	5.06 ± 0.81	17137 ± 80	0.996 ± 0.007	5.31 ± 0.04	35016 ± 85	1.018 ± 0.003	92.68 ± 0.23
	Mean	1765 ± 134	0.94 ± 0.10	3.37 ± 0.59	19270 ± 61	1.00 ± 0.01	4.59 ± 0.03	41341 ± 65	1.01 ± 0.01	89.28 ± 0.15
2959/7	1	468 ± 44	0.921 ± 0.132	2.91 ± 0.47	8880 ± 59	0.983 ± 0.009	14.40 ± 0.11	18661 ± 62	1.063 ± 0.005	142.66 ± 0.48
	2	968 ± 52	0.863 ± 0.073	2.13 ± 0.22	11306 ± 67	1.043 ± 0.009	16.25 ± 0.11	26010 ± 73	1.039 ± 0.004	123.41 ± 0.35
	Mean	718 ± 48	0.89 ± 0.11	2.52 ± 0.37	10093 ± 45	1.01 ± 0.01	15.33 ± 0.11	22335 ± 48	1.05 ± 0.01	133.03 ± 0.30
2959/8	1	640 ± 46	0.763 ± 0.091	1.71 ± 0.24	8012 ± 60	1.005 ± 0.011	3.99 ± 0.05	25606 ± 72	1.029 ± 0.004	95.2 ± 0.28
	2	1357 ± 66	1.008 ± 0.070	4.98 ± 0.38	13820 ± 75	0.992 ± 0.008	7.63 ± 0.06	38213 ± 88	1.002 ± 0.003	98.65 ± 0.23
	Mean	999 ± 57	0.89 ± 0.08	3.34 ± 0.32	10916 ± 48	1.00 ± 0.01	5.81 ± 0.05	31910 ± 57	1.02 ± 0.01	96.93 ± 0.18
2959/9	1	1201 ± 60	1.142 ± 0.080	2.31 ± 0.20	18528 ± 83	1.001 ± 0.006	3.35 ± 0.03	26341 ± 73	1.012 ± 0.004	80.29 ± 0.23
	2	707 ± 50	1.083 ± 0.109	1.65 ± 0.22	7436 ± 56	1.02 ± 0.011	4.56 ± 0.06	17954 ± 61	1.036 ± 0.005	101.26 ± 0.35
	Mean	954 ± 56	1.11 ± 0.10	1.98 ± 0.21	12982 ± 50	1.01 ± 0.01	3.95 ± 0.04	22147 ± 48	1.02 ± 0.01	90.77 ± 0.21

Table B.3: Instrumental profiling results for Monolith Lake (SUTL2960)

SUTL No.	Aliquot	IRSL		OSL		IRSL : OSL
		Net Counts	Depletion	Net Counts	Depletion	
2960/1	1	106 ± 45	2.655 ± 0.409	1919 ± 62	1.130 ± 0.057	0.0552 ± 0.0234
	2	72 ± 44	0.200 ± 0.032	3052 ± 72	1.041 ± 0.042	0.0236 ± 0.0146
	Mean	89 ± 32	1.428 ± 0.205	2486 ± 47	1.086 ± 0.035	0.0394 ± 0.0138
2960/2	1	3061 ± 71	1.247 ± 0.050	78851 ± 285	1.086 ± 0.008	0.0388 ± 0.0009
	2	3651 ± 79	1.293 ± 0.046	115205 ± 345	1.068 ± 0.006	0.0317 ± 0.0007
	Mean	3356 ± 53	1.270 ± 0.034	97028 ± 224	1.077 ± 0.005	0.0353 ± 0.0006
2960/3	1	579 ± 55	1.090 ± 0.093	14080 ± 129	1.143 ± 0.020	0.0411 ± 0.0039
	2	502 ± 53	1.049 ± 0.096	13212 ± 124	1.087 ± 0.019	0.0380 ± 0.0040
	Mean	541 ± 38	1.070 ± 0.067	13646 ± 89	1.115 ± 0.014	0.0396 ± 0.0028
2960/4	1	383 ± 50	1.536 ± 0.156	4634 ± 84	1.236 ± 0.039	0.0826 ± 0.0110
	2	1250 ± 62	1.059 ± 0.065	24898 ± 165	1.171 ± 0.015	0.0502 ± 0.0025
	Mean	817 ± 40	1.298 ± 0.085	14766 ± 92	1.204 ± 0.021	0.0664 ± 0.0056
2960/5	1	792 ± 56	1.118 ± 0.086	12545 ± 121	1.258 ± 0.023	0.0631 ± 0.0045
	2	767 ± 55	1.458 ± 0.110	14466 ± 131	1.276 ± 0.022	0.0530 ± 0.0039
	Mean	780 ± 39	1.288 ± 0.070	13506 ± 89	1.267 ± 0.016	0.0581 ± 0.0030
2960/6	1	10084 ± 111	1.235 ± 0.026	168404 ± 415	1.205 ± 0.006	0.0599 ± 0.0007
	2	22185 ± 158	1.240 ± 0.017	518469 ± 724	1.164 ± 0.003	0.0428 ± 0.0003
	Mean	16135 ± 97	1.237 ± 0.015	343437 ± 417	1.184 ± 0.003	0.0513 ± 0.0004
2960/7	1	38592 ± 204	1.247 ± 0.013	795024 ± 895	1.159 ± 0.003	0.0485 ± 0.0003
	2	120120 ± 352	1.278 ± 0.007	2298087 ± 1521	1.174 ± 0.002	0.0523 ± 0.0002
	Mean	79356 ± 203	1.262 ± 0.007	1546556 ± 883	1.166 ± 0.002	0.0504 ± 0.0002
2960/8	1	149725 ± 391	1.254 ± 0.007	2859426 ± 1697	1.190 ± 0.001	0.0524 ± 0.0001
	2	219655 ± 475	1.273 ± 0.005	4184664 ± 2053	1.182 ± 0.001	0.0525 ± 0.0001
	Mean	184690 ± 308	1.264 ± 0.004	3522045 ± 1332	1.186 ± 0.001	0.0524 ± 0.0001
2960/9	1	88350 ± 302	1.264 ± 0.009	1397774 ± 1188	1.152 ± 0.002	0.0632 ± 0.0002
	2	60685 ± 253	1.457 ± 0.012	1136828 ± 1071	1.160 ± 0.002	0.0534 ± 0.0002
	Mean	74518 ± 197	1.360 ± 0.007	1267301 ± 800	1.156 ± 0.001	0.0583 ± 0.0002
2960/10	1	334366 ± 583	1.276 ± 0.004	5952585 ± 2448	1.387 ± 0.001	0.0562 ± 0.0001
	2	313794 ± 566	1.291 ± 0.005	6259225 ± 2510	1.179 ± 0.001	0.0501 ± 0.0001
	Mean	324080 ± 407	1.284 ± 0.003	6105905 ± 1753	1.283 ± 0.001	0.0532 ± 0.0001
2960/11	1	283397 ± 537	1.304 ± 0.005	5526528 ± 2358	1.218 ± 0.001	0.0513 ± 0.0001
	2	368346 ± 612	1.315 ± 0.004	7273239 ± 2705	1.191 ± 0.001	0.0506 ± 0.0001
	Mean	325872 ± 407	1.309 ± 0.003	6399884 ± 1794	1.204 ± 0.001	0.0510 ± 0.0001
2960/12	1	13562 ± 126	1.325 ± 0.024	207945 ± 460	1.176 ± 0.005	0.0652 ± 0.0006
	2	150421 ± 393	1.289 ± 0.007	2311244 ± 1526	1.189 ± 0.002	0.0651 ± 0.0002
	Mean	81992 ± 206	1.307 ± 0.012	1259595 ± 797	1.182 ± 0.003	0.0652 ± 0.0003
2960/13	1	4911 ± 85	1.299 ± 0.040	70996 ± 272	1.274 ± 0.010	0.0692 ± 0.0012
	2	41225 ± 209	1.284 ± 0.013	519556 ± 725	1.061 ± 0.003	0.0793 ± 0.0004
	Mean	23068 ± 113	1.291 ± 0.021	295276 ± 387	1.167 ± 0.005	0.0743 ± 0.0007
2960/14	1	5851 ± 93	1.287 ± 0.036	72467 ± 276	1.218 ± 0.009	0.0807 ± 0.0013
	2	52999 ± 237	1.282 ± 0.011	673091 ± 825	1.137 ± 0.003	0.0787 ± 0.0004
	Mean	29425 ± 127	1.285 ± 0.019	372779 ± 435	1.177 ± 0.005	0.0797 ± 0.0007
2960/15	1	6949 ± 99	1.283 ± 0.032	107855 ± 335	1.300 ± 0.008	0.0644 ± 0.0009
	2	79463 ± 288	1.313 ± 0.009	990832 ± 1000	1.159 ± 0.002	0.0802 ± 0.0003
	Mean	43206 ± 152	1.298 ± 0.017	549344 ± 527	1.230 ± 0.004	0.0723 ± 0.0005
2960/16	1	5342 ± 89	1.296 ± 0.038	63773 ± 259	1.195 ± 0.010	0.0838 ± 0.0014
	2	50347 ± 231	1.289 ± 0.012	692178 ± 836	1.258 ± 0.003	0.0727 ± 0.0003
	Mean	27845 ± 124	1.292 ± 0.020	377976 ± 437	1.227 ± 0.005	0.0783 ± 0.0007
2960/17	1	8308 ± 104	1.233 ± 0.028	91771 ± 309	1.230 ± 0.008	0.0905 ± 0.0012
	2	25094 ± 168	1.311 ± 0.017	263774 ± 518	1.235 ± 0.005	0.0951 ± 0.0007
	Mean	16701 ± 99	1.272 ± 0.017	177773 ± 301	1.233 ± 0.005	0.0928 ± 0.0007
2960/18	1	7637 ± 102	1.322 ± 0.032	82835 ± 293	1.246 ± 0.009	0.0922 ± 0.0013
	2	23644 ± 162	1.309 ± 0.018	273359 ± 527	1.222 ± 0.005	0.0865 ± 0.0006
	Mean	15641 ± 96	1.316 ± 0.018	178097 ± 301	1.234 ± 0.005	0.0893 ± 0.0007

2960/19	1	4406 ± 85	1.339 ± 0.043	58493 ± 248	1.271 ± 0.011	0.0753 ± 0.0015
	2	39537 ± 206	1.294 ± 0.013	482579 ± 699	1.203 ± 0.003	0.0819 ± 0.0004
	Mean	21972 ± 112	1.316 ± 0.023	270536 ± 371	1.237 ± 0.006	0.0786 ± 0.0008
2960/20	1	5583 ± 90	1.231 ± 0.035	58877 ± 249	1.278 ± 0.011	0.0948 ± 0.0016
	2	53967 ± 239	1.293 ± 0.011	661966 ± 818	1.231 ± 0.003	0.0815 ± 0.0004
	Mean	29775 ± 128	1.262 ± 0.018	360422 ± 427	1.254 ± 0.006	0.0882 ± 0.0008
2960/21	1	4335 ± 85	1.424 ± 0.046	49301 ± 229	1.255 ± 0.011	0.0879 ± 0.0018
	2	21834 ± 158	1.310 ± 0.018	260682 ± 516	1.226 ± 0.005	0.0838 ± 0.0006
	Mean	13085 ± 90	1.367 ± 0.025	154992 ± 282	1.241 ± 0.006	0.0858 ± 0.0009
2960/22	1	3442 ± 78	1.261 ± 0.047	39485 ± 205	1.244 ± 0.013	0.0872 ± 0.0020
	2	23992 ± 164	1.325 ± 0.018	295461 ± 548	1.242 ± 0.005	0.0812 ± 0.0006
	Mean	13717 ± 91	1.293 ± 0.025	167473 ± 293	1.243 ± 0.007	0.0842 ± 0.0011
2960/23	1	7366 ± 101	1.264 ± 0.031	132114 ± 368	1.229 ± 0.007	0.0558 ± 0.0008
	2	61582 ± 255	1.298 ± 0.011	733961 ± 862	1.265 ± 0.003	0.0839 ± 0.0004
	Mean	34474 ± 137	1.281 ± 0.016	433038 ± 469	1.247 ± 0.004	0.0698 ± 0.0004
2960/24	1	8724 ± 107	1.289 ± 0.029	112197 ± 339	1.244 ± 0.007	0.0778 ± 0.0010
	2	72631 ± 275	1.320 ± 0.010	860056 ± 932	1.228 ± 0.003	0.0844 ± 0.0003
	Mean	40678 ± 148	1.305 ± 0.015	486127 ± 496	1.236 ± 0.004	0.0811 ± 0.0005
2960/25	1	7491 ± 101	1.306 ± 0.032	88822 ± 304	1.219 ± 0.008	0.0843 ± 0.0012
	2	53719 ± 238	1.296 ± 0.011	627193 ± 797	1.298 ± 0.003	0.0856 ± 0.0004
	Mean	30605 ± 129	1.301 ± 0.017	358008 ± 426	1.258 ± 0.004	0.0850 ± 0.0006
2960/26	1	4030 ± 82	1.243 ± 0.042	85314 ± 298	1.198 ± 0.008	0.0472 ± 0.0010
	2	68254 ± 268	1.325 ± 0.010	810431 ± 905	1.208 ± 0.003	0.0842 ± 0.0003
	Mean	36142 ± 140	1.284 ± 0.021	447873 ± 476	1.203 ± 0.004	0.0657 ± 0.0005
2960/27	1	16564 ± 139	1.324 ± 0.021	187073 ± 437	1.200 ± 0.006	0.0885 ± 0.0008
	2	166891 ± 414	1.328 ± 0.007	2029636 ± 1430	1.241 ± 0.002	0.0822 ± 0.0002
	Mean	91728 ± 218	1.326 ± 0.011	1108355 ± 748	1.220 ± 0.003	0.0854 ± 0.0004
2960/28	1	25436 ± 168	1.313 ± 0.017	338629 ± 586	1.247 ± 0.004	0.0751 ± 0.0005
	2	158224 ± 403	1.352 ± 0.007	1983820 ± 1414	1.217 ± 0.002	0.0798 ± 0.0002
	Mean	91830 ± 218	1.332 ± 0.009	1161225 ± 765	1.232 ± 0.002	0.0774 ± 0.0003
2960/29	1	48206 ± 228	1.336 ± 0.012	611238 ± 786	1.201 ± 0.003	0.0789 ± 0.0004
	2	210637 ± 464	1.320 ± 0.006	3113449 ± 1771	1.183 ± 0.001	0.0677 ± 0.0002
	Mean	129422 ± 258	1.328 ± 0.007	1862344 ± 969	1.192 ± 0.002	0.0733 ± 0.0002
2960/30	1	62388 ± 255	1.288 ± 0.010	846890 ± 925	1.192 ± 0.003	0.0737 ± 0.0003
	2	95250 ± 314	1.291 ± 0.008	1172696 ± 1088	1.132 ± 0.002	0.0812 ± 0.0003
	Mean	78819 ± 203	1.290 ± 0.007	1009793 ± 714	1.162 ± 0.002	0.0774 ± 0.0002
2960/31	1	99848 ± 321	1.313 ± 0.008	1362443 ± 1171	1.194 ± 0.002	0.0733 ± 0.0002
	2	208693 ± 462	1.296 ± 0.006	3049271 ± 1753	1.175 ± 0.001	0.0684 ± 0.0002
	Mean	154271 ± 281	1.305 ± 0.005	2205857 ± 1054	1.184 ± 0.001	0.0709 ± 0.0001

Table B.4: Profiling results for Monolith Lake (SUTL2960)

SUTL No.	Aliquot	Quartz (OSL)			Polymineral (IRSL)			Polymineral (TL)		
		Sensitivity (c Gy^{-1})	Sensitivity change	Ed (Gy)	Sensitivity (c Gy^{-1})	Sensitivity change	Ed (Gy)	Sensitivity (c Gy^{-1})	Sensitivity change	Ed (Gy)
2960/1	1	245 ± 34	0.547 ± 0.165	0.21 ± 0.18	793 ± 22	1.171 ± 0.05	1.11 ± 0.11			
	2	254 ± 37	1.352 ± 0.255	0.88 ± 0.24	3372 ± 41	0.945 ± 0.016	1.07 ± 0.04	1897 ± 20	1.060 ± 0.016	157.33 ± 1.66
	Mean	245 ± 25	0.95 ± 0.15	0.54 ± 0.15	793 ± 23	1.06 ± 0.03	1.09 ± 0.06	1897 ± 20	1.06 ± 0.02	157.33 ± 1.66
2960/2	1	641 ± 50	1.154 ± 0.124	1.10 ± 0.18	5479 ± 47	1.042 ± 0.013	1.85 ± 0.04	5395 ± 33	0.975 ± 0.008	146.20 ± 0.91
	2	260 ± 42	0.861 ± 0.230	0.89 ± 0.35	2531 ± 33	0.985 ± 0.018	1.53 ± 0.06	6650 ± 37	1.088 ± 0.009	48.59 ± 0.28
	Mean	641 ± 33	1.01 ± 0.13	0.99 ± 0.19	5479 ± 29	1.01 ± 0.01	1.69 ± 0.03	5395 ± 25	1.03 ± 0.01	97.40 ± 0.48
2960/3	1	257 ± 42	1.458 ± 0.297	1.63 ± 0.44	2210 ± 33	0.993 ± 0.021	6.09 ± 0.13	4945 ± 32	1.025 ± 0.009	100.57 ± 0.66
	2	241 ± 40	1.752 ± 0.351	1.87 ± 0.45	3935 ± 42	0.988 ± 0.015	5.23 ± 0.08	7024 ± 38	1.043 ± 0.008	93.79 ± 0.52
	Mean	257 ± 29	1.60 ± 0.23	1.75 ± 0.31	2210 ± 26	0.99 ± 0.01	5.66 ± 0.08	4945 ± 25	1.03 ± 0.01	97.18 ± 0.42
2960/4	1	209 ± 38	0.923 ± 0.274	-0.01 ± -0.16	3455 ± 39	0.949 ± 0.015	2.20 ± 0.05	8255 ± 41	1.017 ± 0.007	57.95 ± 0.30
	2	123 ± 33	1.200 ± 0.426	0.70 ± 0.56	2145 ± 32	0.998 ± 0.021	2.42 ± 0.07	8269 ± 41	0.975 ± 0.007	39.97 ± 0.21
	Mean	209 ± 25	1.06 ± 0.25	0.34 ± 0.29	3455 ± 25	0.97 ± 0.01	2.31 ± 0.04	8255 ± 29	1.00 ± 0.01	48.96 ± 0.18
2960/5	1	79 ± 33	1.639 ± 0.797	0.15 ± 0.48	6315 ± 51	0.979 ± 0.011	1.57 ± 0.03	6052 ± 35	0.999 ± 0.008	74.82 ± 0.45
	2	518 ± 46	0.939 ± 0.126	1.89 ± 0.30	1826 ± 30	0.984 ± 0.023	1.67 ± 0.06	9979 ± 45	0.983 ± 0.006	27.09 ± 0.13
	Mean	79 ± 28	1.29 ± 0.4	1.02 ± 0.28	6315 ± 30	0.98 ± 0.01	1.62 ± 0.04	6052 ± 29	0.99 ± 0.01	50.95 ± 0.23
2960/6	1	1281 ± 69	0.992 ± 0.075	7.49 ± 0.61	12897 ± 72	1.037 ± 0.008	18.94 ± 0.12	4905 ± 32	1.013 ± 0.009	573.77 ± 3.72
	2	794 ± 55	0.919 ± 0.096	10.17 ± 1.12	6091 ± 51	1.006 ± 0.012	18.27 ± 0.18	18065 ± 61	1.037 ± 0.005	93.15 ± 0.32
	Mean	1281 ± 44	0.96 ± 0.06	8.83 ± 0.64	12897 ± 44	1.02 ± 0.01	18.61 ± 0.11	4905 ± 34	1.03 ± 0.01	333.46 ± 1.87
2960/7	1	3070 ± 111	0.813 ± 0.046	8.33 ± 0.51	6540 ± 53	1.064 ± 0.012	34.41 ± 0.30	12658 ± 51	0.992 ± 0.006	313.62 ± 1.27
	2	5228 ± 133	1.000 ± 0.036	12.05 ± 0.46	12947 ± 72	1.034 ± 0.008	39.41 ± 0.24	15451 ± 56	1.065 ± 0.006	610.17 ± 2.23
	Mean	3070 ± 87	0.91 ± 0.03	10.19 ± 0.34	6540 ± 45	1.05 ± 0.01	36.91 ± 0.19	12658 ± 38	1.03 ± 0.01	461.89 ± 1.28
2960/8	1	4978 ± 123	0.828 ± 0.031	7.05 ± 0.28	5875 ± 50	1.044 ± 0.013	44.81 ± 0.41	29692 ± 78	1.100 ± 0.004	132.73 ± 0.35
	2	4456 ± 118	0.822 ± 0.033	7.79 ± 0.36	9177 ± 61	1.087 ± 0.011	40.71 ± 0.29	13186 ± 52	1.075 ± 0.006	409.30 ± 1.62
	Mean	4978 ± 85	0.82 ± 0.02	7.42 ± 0.23	5875 ± 40	1.07 ± 0.01	42.76 ± 0.25	29692 ± 47	1.09 ± 0.01	271.01 ± 0.83
2960/9	1	3216 ± 102	0.869 ± 0.041	7.72 ± 0.41	10820 ± 64	1.022 ± 0.009	36.59 ± 0.23	18174 ± 61	1.050 ± 0.005	364.19 ± 1.23
	2	1285 ± 76	0.980 ± 0.082	8.65 ± 0.81	7111 ± 55	1.061 ± 0.012	47.66 ± 0.39	24395 ± 71	1.067 ± 0.004	213.75 ± 0.63
	Mean	3216 ± 64	0.92 ± 0.05	8.19 ± 0.45	10820 ± 42	1.04 ± 0.01	42.13 ± 0.23	18174 ± 47	1.06 ± 0.01	288.97 ± 0.69
2960/10	1	1953 ± 81	0.739 ± 0.05	7.16 ± 0.53	9196 ± 61	1.016 ± 0.01	40.22 ± 0.29	19226 ± 63	1.085 ± 0.005	298.23 ± 0.98
	2	2282 ± 96	0.898 ± 0.055	7.28 ± 0.48	10823 ± 65	1.066 ± 0.009	39.42 ± 0.26	21399 ± 66	1.066 ± 0.005	385.77 ± 1.20
	Mean	1953 ± 63	0.82 ± 0.04	7.22 ± 0.36	9196 ± 45	1.04 ± 0.01	39.82 ± 0.19	19226 ± 46	1.08 ± 0.01	342.00 ± 0.77

2960/11	1	4295 ± 133	0.890 ± 0.041	8.54 ± 0.42	14250 ± 75	0.970 ± 0.007	31.01 ± 0.18	29921 ± 78	1.045 ± 0.004	301.98 ± 0.80
	2	4152 ± 273	0.709 ± 0.079	6.05 ± 0.70	18976 ± 87	0.986 ± 0.006	40.86 ± 0.20	33902 ± 83	1.099 ± 0.004	276.49 ± 0.68
	Mean	4295 ± 152	0.80 ± 0.04	7.30 ± 0.41	14250 ± 57	0.98 ± 0.01	35.93 ± 0.13	29921 ± 57	1.07 ± 0.01	289.24 ± 0.52
2960/12	1	3772 ± 121	0.762 ± 0.039	9.69 ± 0.53	9435 ± 61	1.044 ± 0.010	46.24 ± 0.32	34558 ± 84	1.061 ± 0.004	188.94 ± 0.47
	2	3024 ± 107	0.828 ± 0.045	8.16 ± 0.48	5117 ± 46	1.021 ± 0.013	63.51 ± 0.61	23379 ± 69	1.080 ± 0.005	206.68 ± 0.62
	Mean	3772 ± 81	0.79 ± 0.03	8.93 ± 0.36	9435 ± 39	1.03 ± 0.01	54.88 ± 0.34	34558 ± 54	1.07 ± 0.01	197.81 ± 0.39
2960/13	1	1531 ± 79	0.916 ± 0.068	9.76 ± 0.79	4395 ± 46	0.962 ± 0.014	40.74 ± 0.45	11897 ± 49	1.053 ± 0.006	264.91 ± 1.11
	2	647 ± 57	0.853 ± 0.110	6.58 ± 0.93	3038 ± 37	0.979 ± 0.017	25.13 ± 0.34	8437 ± 42	0.995 ± 0.007	209.95 ± 1.05
	Mean	1531 ± 48	0.88 ± 0.06	8.17 ± 0.61	4395 ± 29	0.97 ± 0.01	32.94 ± 0.28	11897 ± 32	1.02 ± 0.01	237.43 ± 0.76
2960/14	1	2044 ± 86	0.683 ± 0.049	7.97 ± 0.62	6152 ± 51	0.971 ± 0.011	28.04 ± 0.26	12765 ± 51	1.054 ± 0.006	244.38 ± 0.99
	2	2532 ± 101	0.906 ± 0.052	11.02 ± 0.69	7219 ± 55	1.032 ± 0.011	31.42 ± 0.26	21399 ± 66	1.018 ± 0.004	250.82 ± 0.78
	Mean	2044 ± 66	0.79 ± 0.04	9.49 ± 0.46	6152 ± 37	1.00 ± 0.01	29.73 ± 0.18	12765 ± 42	1.04 ± 0.01	247.60 ± 0.63
2960/15	1	1844 ± 83	0.862 ± 0.058	10.29 ± 0.73	1669 ± 29	0.971 ± 0.023	115.35 ± 2.03	3466 ± 27	1.062 ± 0.012	344.36 ± 2.66
	2	990 ± 71	0.913 ± 0.095	9.27 ± 1.03	1115 ± 25	1.014 ± 0.033	40.74 ± 0.99	2517 ± 23	0.983 ± 0.012	249.28 ± 2.27
	Mean	1844 ± 55	0.89 ± 0.06	9.78 ± 0.63	1669 ± 19	0.99 ± 0.02	78.04 ± 1.13	3466 ± 17	1.02 ± 0.01	296.82 ± 1.75
2960/16	1	1426 ± 82	1.091 ± 0.086	10.62 ± 0.90	2686 ± 35	0.962 ± 0.018	31.01 ± 0.44	8726 ± 42	1.059 ± 0.007	219.95 ± 1.08
	2	2601 ± 106	0.792 ± 0.050	8.21 ± 0.57	3484 ± 38	0.992 ± 0.015	19.78 ± 0.24	9013 ± 43	1.041 ± 0.007	213.31 ± 1.03
	Mean	1426 ± 67	0.94 ± 0.05	9.42 ± 0.53	2686 ± 26	0.98 ± 0.01	25.40 ± 0.25	8726 ± 30	1.05 ± 0.01	216.63 ± 0.74
2960/17	1	4188 ± 116	0.835 ± 0.035	10.73 ± 0.49	10814 ± 66	1.015 ± 0.009	22.40 ± 0.16	27945 ± 76	1.044 ± 0.004	225.50 ± 0.62
	2	1377 ± 78	0.850 ± 0.072	9.95 ± 0.92	5936 ± 51	1.014 ± 0.012	39.93 ± 0.37	21079 ± 66	1.031 ± 0.005	318.10 ± 1.00
	Mean	4188 ± 70	0.84 ± 0.04	10.34 ± 0.52	10814 ± 42	1.01 ± 0.01	31.17 ± 0.20	27945 ± 50	1.04 ± 0.01	271.80 ± 0.59
2960/18	1	2924 ± 114	0.881 ± 0.050	9.94 ± 0.60	4772 ± 44	0.986 ± 0.013	24.59 ± 0.25	8797 ± 42	1.027 ± 0.007	244.78 ± 1.19
	2	2594 ± 126	0.699 ± 0.056	8.60 ± 0.73	7414 ± 56	1.006 ± 0.011	26.54 ± 0.22	18454 ± 61	1.028 ± 0.005	267.37 ± 0.90
	Mean	2924 ± 85	0.79 ± 0.04	9.27 ± 0.47	4772 ± 36	1.00 ± 0.01	25.57 ± 0.17	8797 ± 37	1.03 ± 0.01	256.08 ± 0.75
2960/19	1	3890 ± 113	0.724 ± 0.035	6.38 ± 0.33	4525 ± 43	1.023 ± 0.014	29.55 ± 0.31	11946 ± 49	1.012 ± 0.006	252.64 ± 1.06
	2	4374 ± 129	0.844 ± 0.037	10.00 ± 0.47	6122 ± 51	1.006 ± 0.012	24.10 ± 0.22	8394 ± 41	1.050 ± 0.007	211.79 ± 1.06
	Mean	3890 ± 86	0.78 ± 0.03	8.19 ± 0.29	4525 ± 33	1.01 ± 0.01	26.83 ± 0.19	11946 ± 32	1.03 ± 0.01	232.22 ± 0.75
2960/20	1	2008 ± 85	0.956 ± 0.059	7.84 ± 0.54	9040 ± 59	1.014 ± 0.009	19.65 ± 0.15	15490 ± 56	1.054 ± 0.005	199.24 ± 0.73
	2	3369 ± 110	0.704 ± 0.038	8.15 ± 0.48	4766 ± 45	0.998 ± 0.013	19.29 ± 0.21	13539 ± 53	1.043 ± 0.006	277.46 ± 1.09
	Mean	2008 ± 70	0.83 ± 0.03	7.99 ± 0.36	9040 ± 37	1.01 ± 0.01	19.47 ± 0.13	15490 ± 39	1.05 ± 0.01	238.35 ± 0.66
2960/21	1	2791 ± 106	0.782 ± 0.045	7.88 ± 0.53	5898 ± 48	0.971 ± 0.011	20.43 ± 0.19	15399 ± 56	1.044 ± 0.005	237.85 ± 0.88
	2	2255 ± 96	0.726 ± 0.050	7.52 ± 0.57	6091 ± 49	0.989 ± 0.011	25.10 ± 0.22	9873 ± 45	1.063 ± 0.007	228.73 ± 1.05
	Mean	2791 ± 71	0.75 ± 0.03	7.70 ± 0.39	5898 ± 34	0.98 ± 0.01	22.77 ± 0.15	15399 ± 36	1.05 ± 0.01	233.29 ± 0.68

2960/22	1	3846 ± 124	0.938 ± 0.044	9.69 ± 0.49	2275 ± 32	0.980 ± 0.019	41.23 ± 0.61	5632 ± 34	1.011 ± 0.009	280.16 ± 1.70
	2	2230 ± 89	0.656 ± 0.045	7.30 ± 0.56	2869 ± 35	0.982 ± 0.017	30.44 ± 0.41	8257 ± 41	1.017 ± 0.007	204.00 ± 1.03
	Mean	3846 ± 76	0.80 ± 0.03	8.50 ± 0.37	2275 ± 24	0.98 ± 0.01	35.84 ± 0.37	5632 ± 27	1.01 ± 0.01	242.08 ± 0.99
2960/23	1	1913 ± 85	0.881 ± 0.057	8.76 ± 0.63	3843 ± 40	0.955 ± 0.014	13.37 ± 0.17	6694 ± 37	1.049 ± 0.008	173.42 ± 0.97
	2	1031 ± 66	0.966 ± 0.09	7.28 ± 0.77	2626 ± 32	0.993 ± 0.017	23.64 ± 0.32	4931 ± 32	0.989 ± 0.009	259.38 ± 1.69
	Mean	1913 ± 54	0.92 ± 0.05	8.02 ± 0.50	3843 ± 26	0.97 ± 0.01	18.50 ± 0.18	6694 ± 24	1.02 ± 0.01	216.40 ± 0.97
2960/24	1	1352 ± 78	0.918 ± 0.077	7.89 ± 0.72	1120 ± 24	0.982 ± 0.03	26.68 ± 0.63	3596 ± 27	1.017 ± 0.011	240.18 ± 1.83
	2	2719 ± 102	0.952 ± 0.051	11.03 ± 0.63	1572 ± 27	1.039 ± 0.026	23.92 ± 0.46	3791 ± 28	0.982 ± 0.010	231.51 ± 1.72
	Mean	1352 ± 64	0.93 ± 0.05	9.46 ± 0.48	1120 ± 18	1.01 ± 0.02	25.30 ± 0.39	3596 ± 19	1.00 ± 0.01	235.84 ± 1.25
2960/25	1	1870 ± 84	1.001 ± 0.062	10.17 ± 0.70	6135 ± 49	0.975 ± 0.011	17.31 ± 0.16	12043 ± 50	1.032 ± 0.006	179.55 ± 0.75
	2	2923 ± 97	0.752 ± 0.041	8.29 ± 0.48	4872 ± 43	1.010 ± 0.013	19.63 ± 0.20	6211 ± 36	0.994 ± 0.008	237.90 ± 1.38
	Mean	1870 ± 64	0.88 ± 0.04	9.23 ± 0.42	6135 ± 33	0.99 ± 0.01	18.47 ± 0.13	12043 ± 31	1.01 ± 0.01	208.72 ± 0.78
2960/26	1	6788 ± 200	0.829 ± 0.036	7.22 ± 0.34	9909 ± 64	0.994 ± 0.009	23.01 ± 0.17	22980 ± 69	1.004 ± 0.004	199.91 ± 0.60
	2	3089 ± 105	0.851 ± 0.044	8.90 ± 0.49	13207 ± 73	0.988 ± 0.008	21.52 ± 0.13	22400 ± 68	1.026 ± 0.004	207.64 ± 0.63
	Mean	6788 ± 113	0.84 ± 0.03	8.06 ± 0.30	9909 ± 48	0.99 ± 0.01	22.27 ± 0.11	22980 ± 48	1.01 ± 0.01	203.77 ± 0.44
2960/27	1	5298 ± 146	0.825 ± 0.035	9.21 ± 0.41	8488 ± 57	0.938 ± 0.009	21.70 ± 0.16	13218 ± 52	0.989 ± 0.005	260.57 ± 1.03
	2	5255 ± 137	0.810 ± 0.033	8.06 ± 0.35	3064 ± 37	0.989 ± 0.017	29.64 ± 0.39	7906 ± 40	1.013 ± 0.007	195.52 ± 1.01
	Mean	5298 ± 100	0.82 ± 0.02	8.64 ± 0.27	8488 ± 34	0.96 ± 0.01	25.67 ± 0.21	13218 ± 33	1.00 ± 0.01	228.04 ± 0.72
2960/28	1	9124 ± 211	0.898 ± 0.031	6.17 ± 0.22	3506 ± 40	0.988 ± 0.016	34.08 ± 0.42	9979 ± 45	1.019 ± 0.007	222.01 ± 1.02
	2	8692 ± 293	0.700 ± 0.040	5.13 ± 0.30	6789 ± 51	0.972 ± 0.01	21.96 ± 0.19	13250 ± 52	1.014 ± 0.006	240.52 ± 0.95
	Mean	9124 ± 181	0.80 ± 0.03	5.65 ± 0.19	3506 ± 33	0.98 ± 0.01	28.02 ± 0.23	9979 ± 34	1.02 ± 0.01	231.26 ± 0.70
2960/29	1	25610 ± 581	0.635 ± 0.026	7.05 ± 0.30	5903 ± 50	1.001 ± 0.012	41.33 ± 0.38	12468 ± 50	1.036 ± 0.006	319.70 ± 1.30
	2	27524 ± 678	0.678 ± 0.029	6.83 ± 0.30	4460 ± 43	0.976 ± 0.013	31.94 ± 0.34	9217 ± 43	1.084 ± 0.007	305.96 ± 1.45
	Mean	25610 ± 446	0.66 ± 0.02	6.94 ± 0.21	5903 ± 33	0.99 ± 0.01	36.64 ± 0.25	12468 ± 33	1.06 ± 0.01	312.83 ± 0.98
2960/30	1	8341 ± 189	0.829 ± 0.028	7.45 ± 0.28	13441 ± 72	0.986 ± 0.007	31.12 ± 0.18	31266 ± 80	1.027 ± 0.004	298.70 ± 0.77
	2	20995 ± 481	0.597 ± 0.024	7.54 ± 0.32	7694 ± 55	1.007 ± 0.010	31.05 ± 0.24	20893 ± 65	1.014 ± 0.005	261.85 ± 0.83
	Mean	8341 ± 258	0.71 ± 0.02	7.50 ± 0.21	13441 ± 45	1.00 ± 0.01	31.09 ± 0.15	31266 ± 52	1.02 ± 0.01	280.28 ± 0.56
2960/31	1	7963 ± 181	0.727 ± 0.027	7.13 ± 0.28	4427 ± 43	1.033 ± 0.014	24.12 ± 0.26	13463 ± 52	1.078 ± 0.006	252.80 ± 0.99
	2	33941 ± 466	0.678 ± 0.015	7.81 ± 0.19	15695 ± 77	1.007 ± 0.007	26.93 ± 0.15	29043 ± 77	1.014 ± 0.004	292.19 ± 0.78
	Mean	7963 ± 250	0.70 ± 0.02	7.47 ± 0.17	4427 ± 44	1.02 ± 0.01	25.53 ± 0.15	13463 ± 47	1.05 ± 0.01	272.49 ± 0.63

Appendix C: Dose response curves

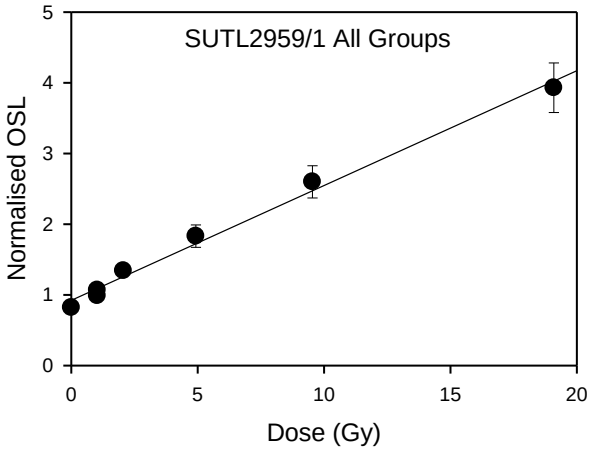

Figure C.1: Dose response curve for SUTL2959/1, average for all accepted aliquots.

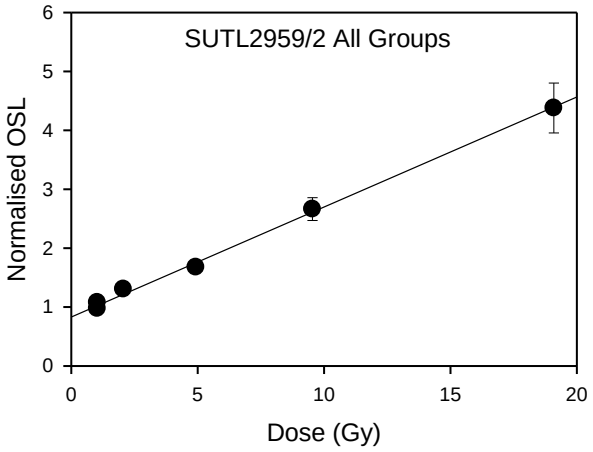

Figure C.2: Dose response curve for SUTL2959/2, average for all accepted aliquots.

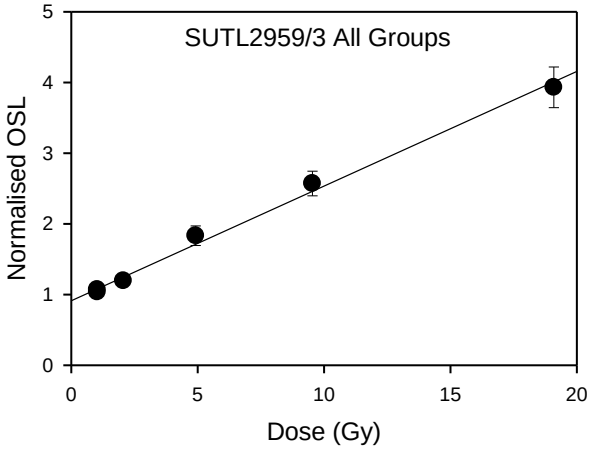

Figure C.3: Dose response curve for SUTL2959/3, average for all accepted aliquots.

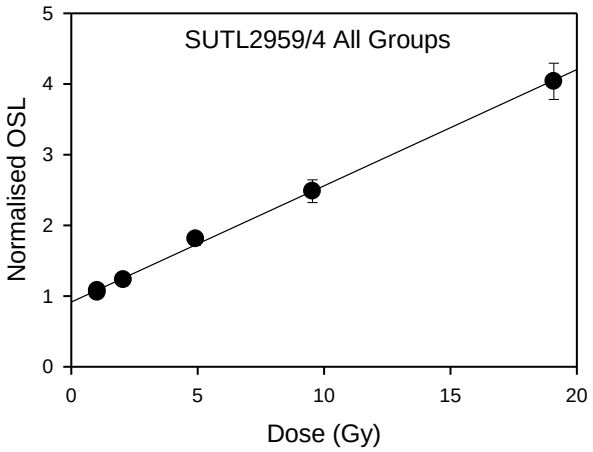

Figure C.4: Dose response curve for SUTL2959/4, average for all accepted aliquots.

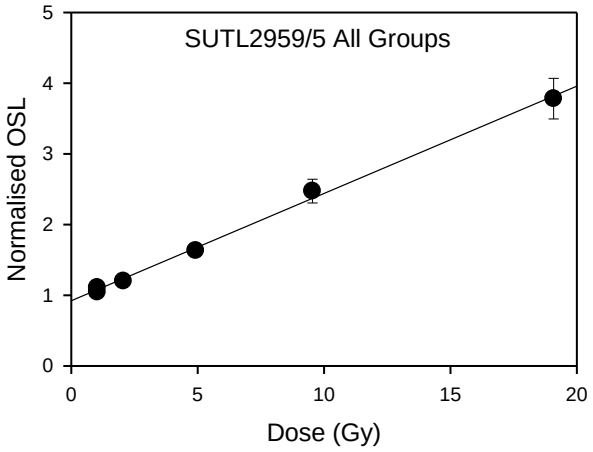

Figure C.5: Dose response curve for SUTL2959/5, average for all accepted aliquots.

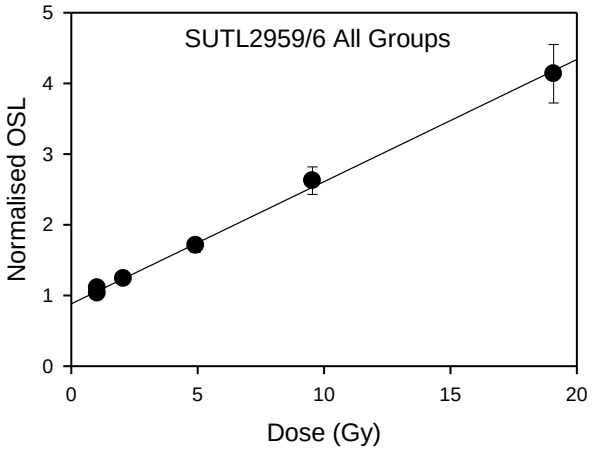

Figure C.6: Dose response curve for SUTL2959/6, average for all accepted aliquots.

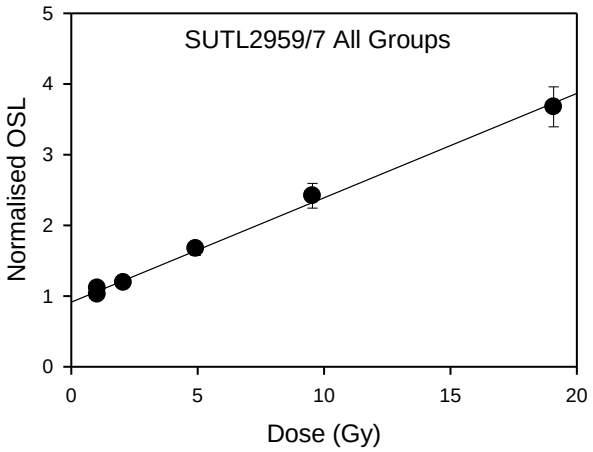

Figure C.7: Dose response curve for SUTL2959/7, average for all accepted aliquots.

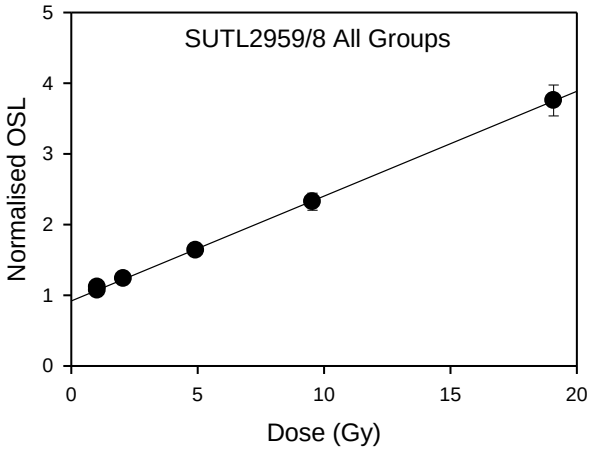

Figure C.8: Dose response curve for SUTL2959/8, average for all accepted aliquots.

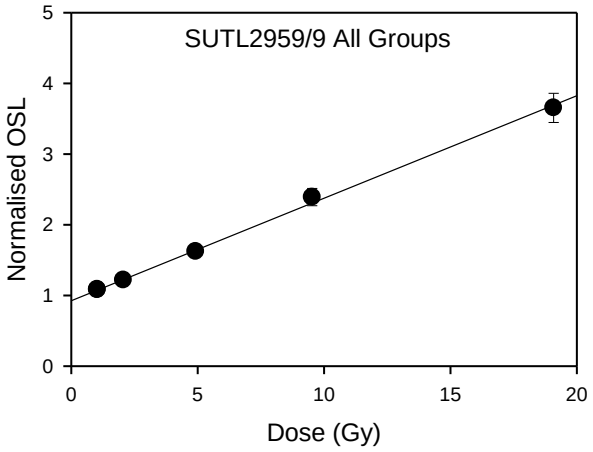

Figure C.9: Dose response curve for SUTL2959/9, average for all accepted aliquots.

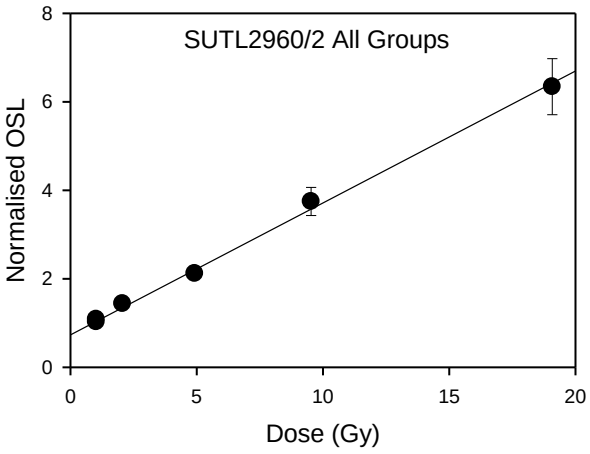

Figure C.10: Dose response curve for SUTL2960/2, average for all accepted aliquots.

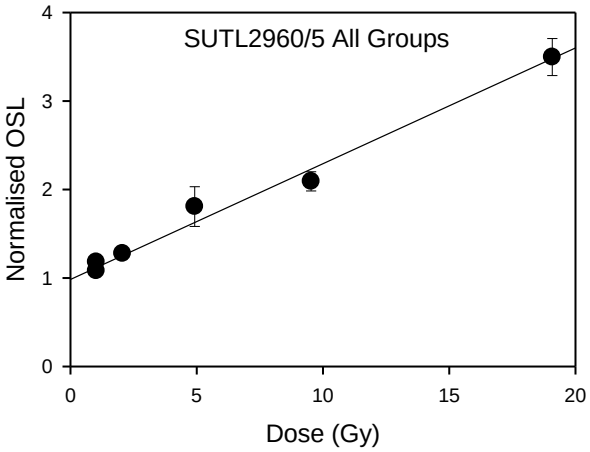

Figure C.11: Dose response curve for SUTL2960/5, average for all accepted aliquots.

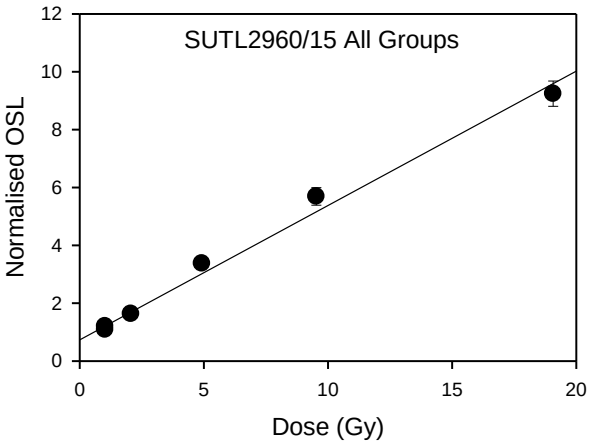

Figure C.12: Dose response curve for SUTL2960/15, average for all accepted aliquots.

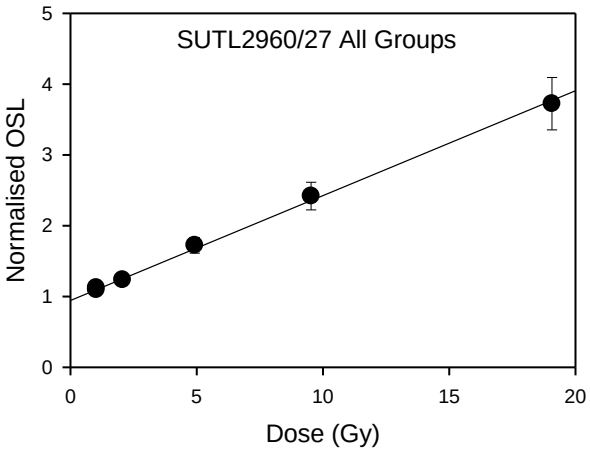

Figure C.13: Dose response curve for SUTL2960/27, average for all accepted aliquots.

Appendix D: Dose Distribution Plots

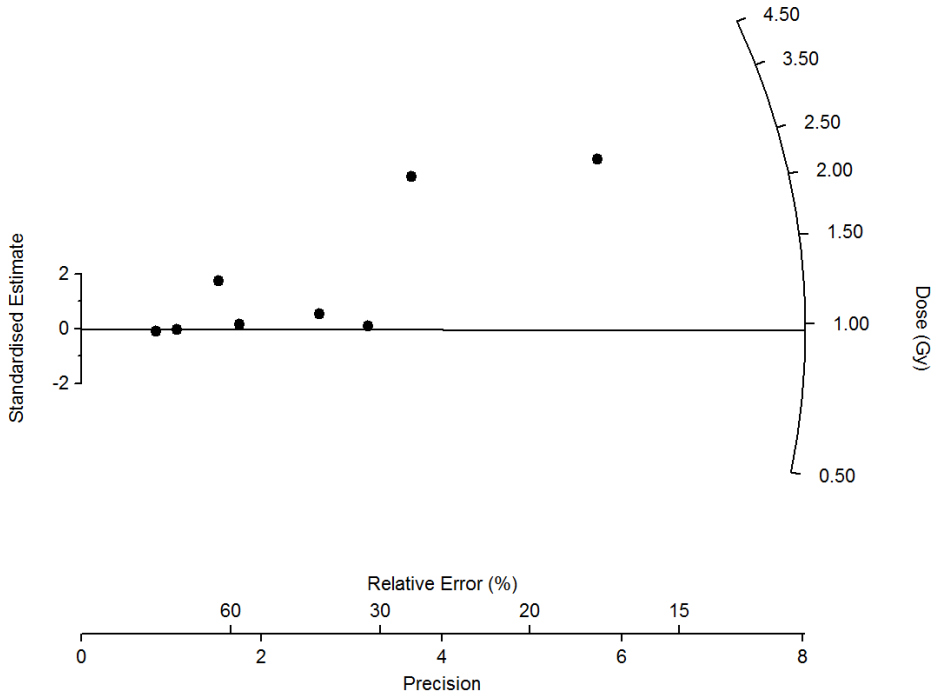

Figure D.1: Radial plot for SUTL2959/1. The line indicates the weighted mean.

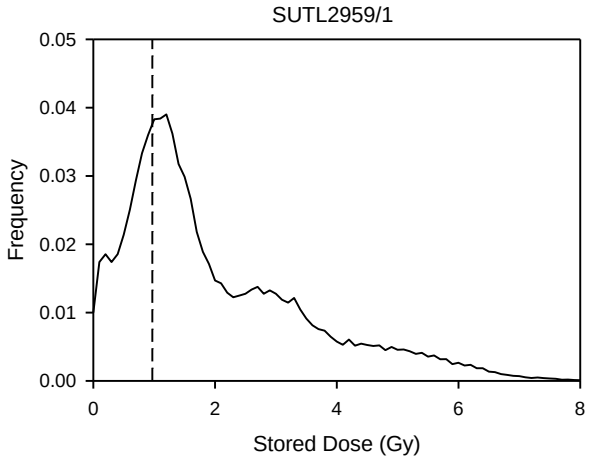

Figure D.2: Probability distribution plot for SUTL2959/1. The dashed line indicates the weighted mean.

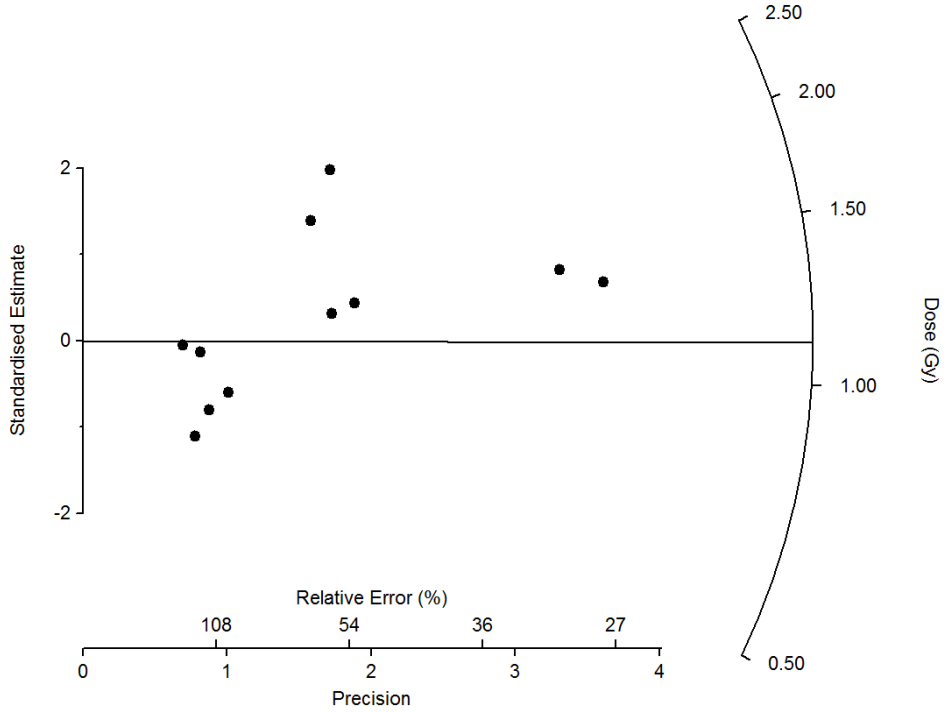

Figure D.3: Radial plot for SUTL2959/2. The line indicates the robust mean.

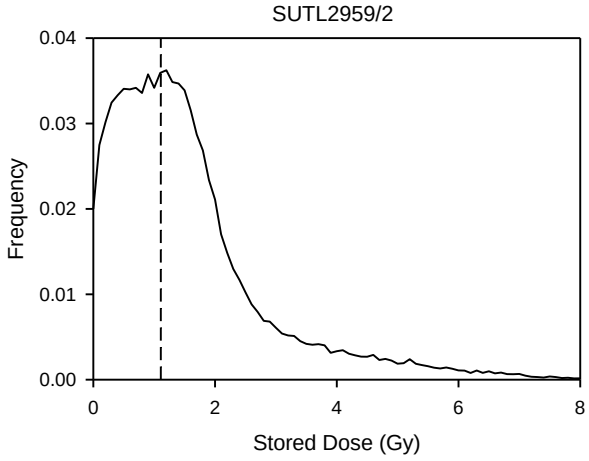

Figure D.4: Probability distribution plot for SUTL2959/2. The dashed line indicates the robust mean.

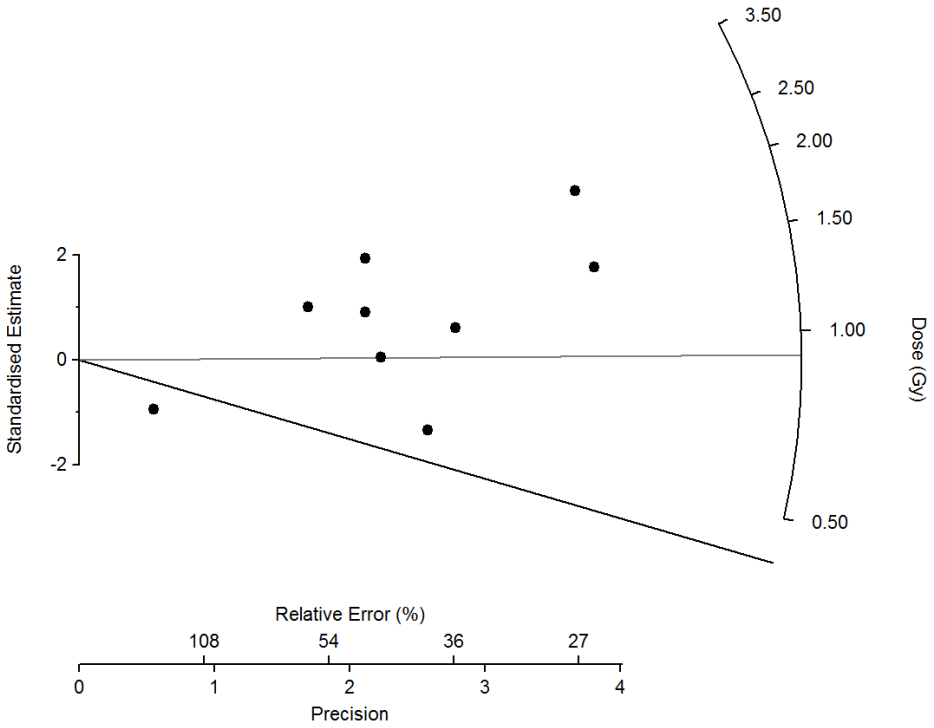

Figure D.5: Radial plot for SUTL2959/3. The black line indicates the weighted mean, with the grey line indicating the robust mean.

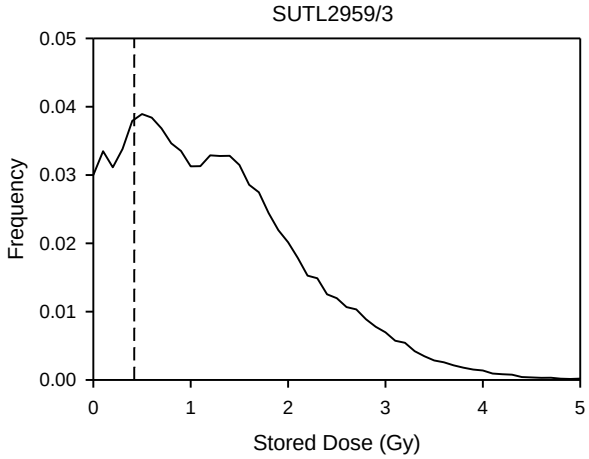

Figure D.6: Probability distribution plot for SUTL2959/3. The dashed line indicates the weighted mean.

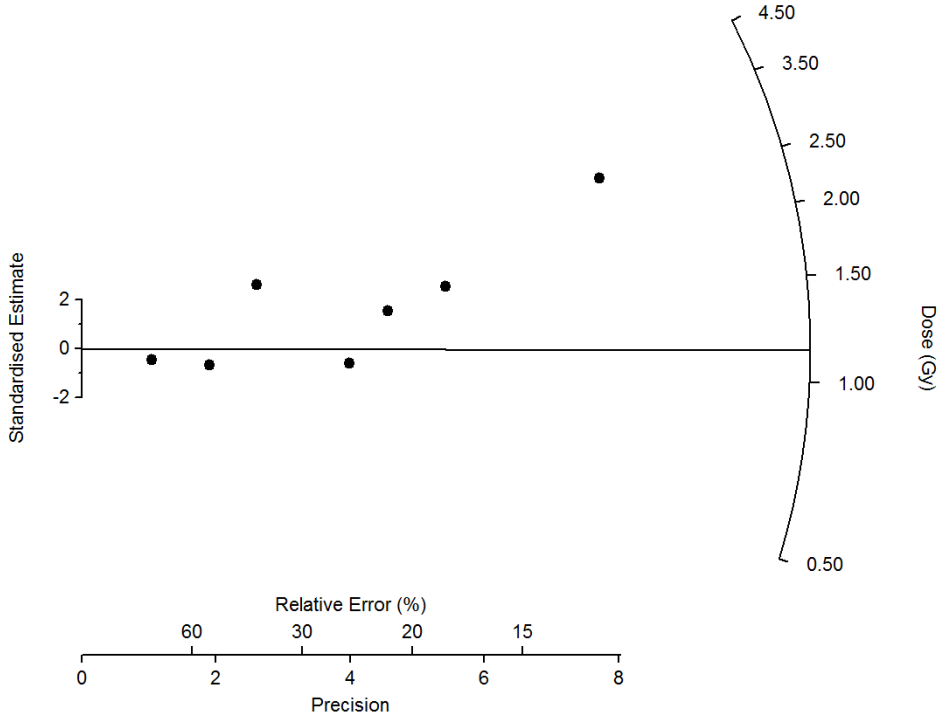

Figure D.7: Radial plot for SUTL2959/4. The line indicates the weighted mean.

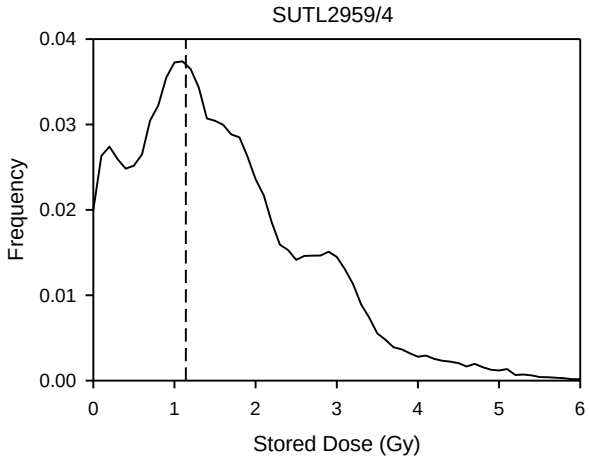

Figure D.8: Probability distribution plot for SUTL2959/4. The dashed line indicates the weighted mean.

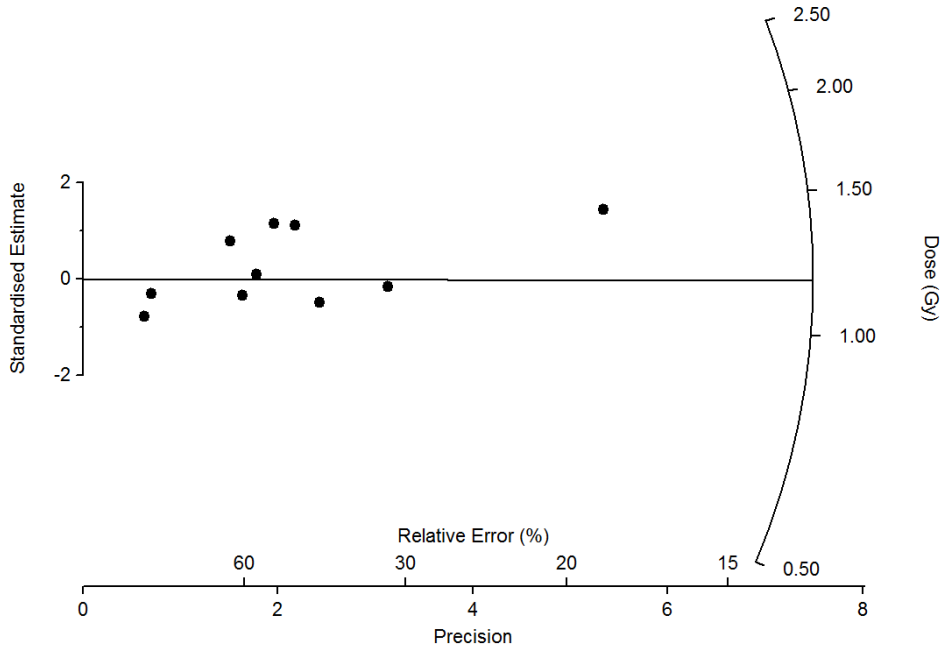

Figure D.9: Radial plot for SUTL2959/5. The line indicates the robust mean.

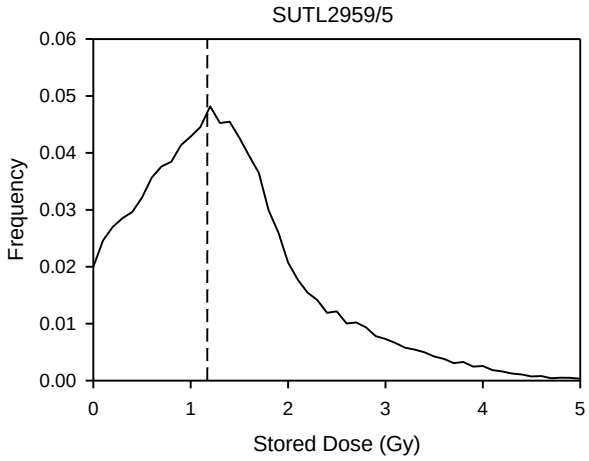

Figure D.10: Probability distribution plot for SUTL2959/5. The dashed line indicates the robust mean.

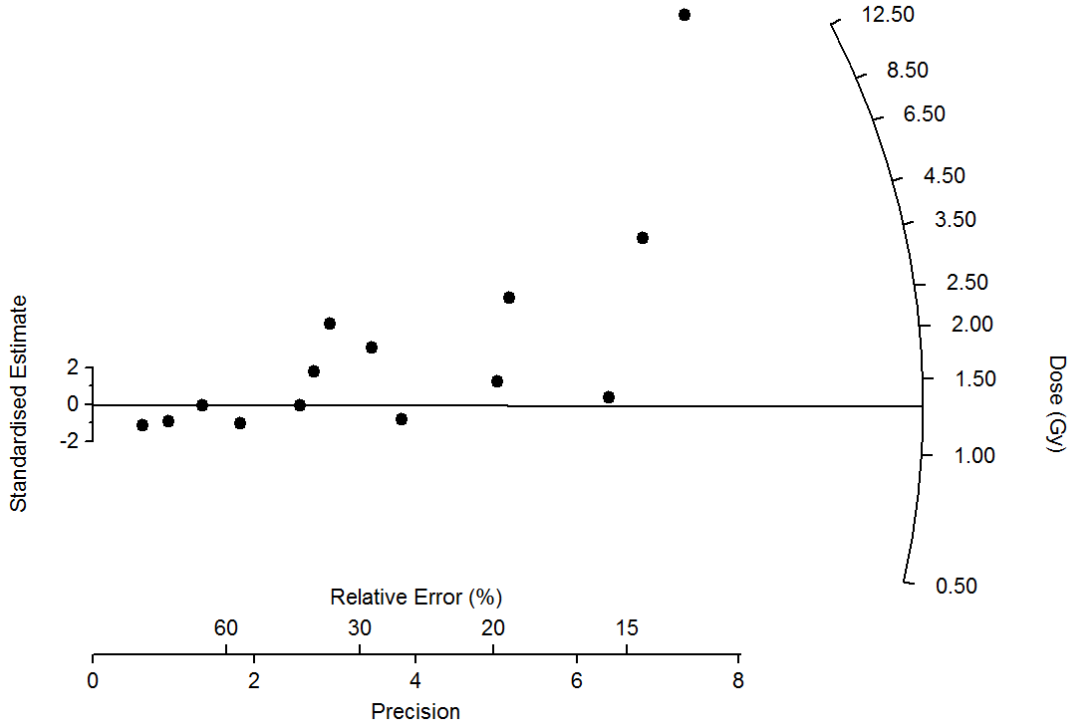

Figure D.11: Radial plot for SUTL2959/6. The line indicates the weighted mean.

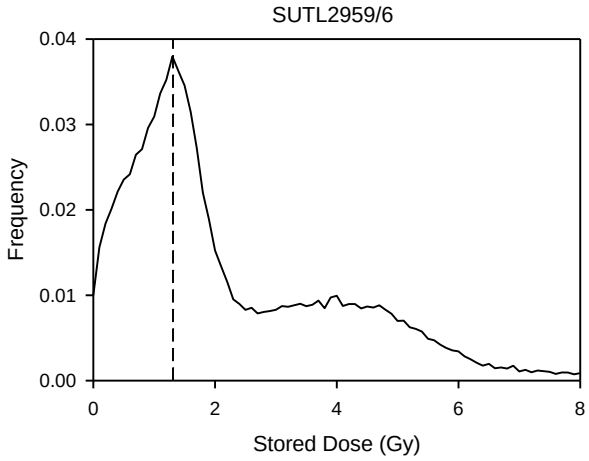

Figure D.12: Probability distribution plot for SUTL2959/6. The dashed line indicates the weighted mean.

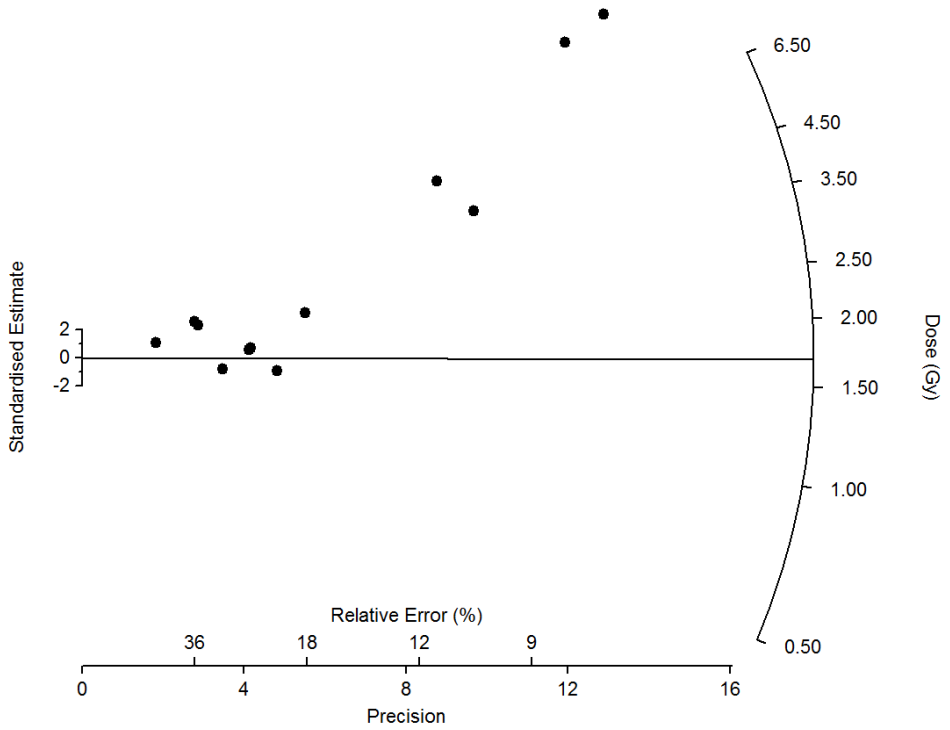

Figure D.13: Radial plot for SUTL2959/7. The line indicates the weighted mean for the lower dose component.

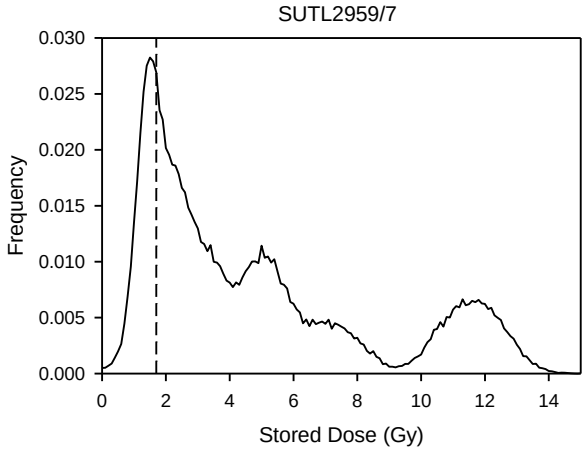

Figure D.14: Probability distribution plot for SUTL2959/7. The dashed line indicates the weighted mean for the lowest dose peak.

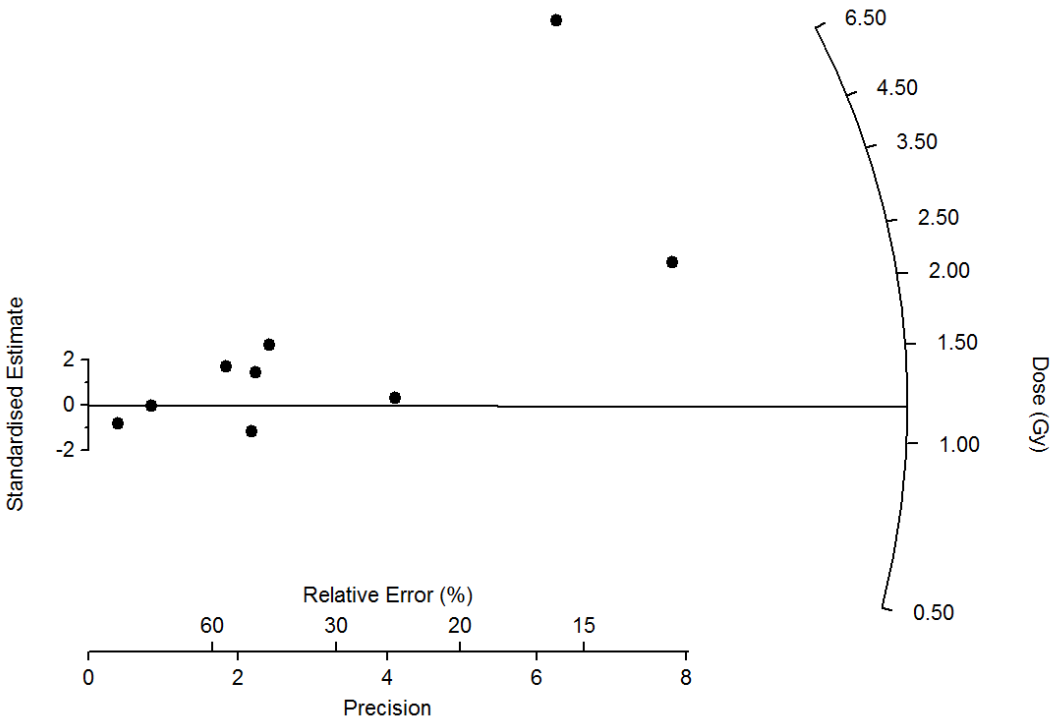

Figure D.15: Abanico plot for SUTL2959/8. The dashed line indicates the weighted mean.

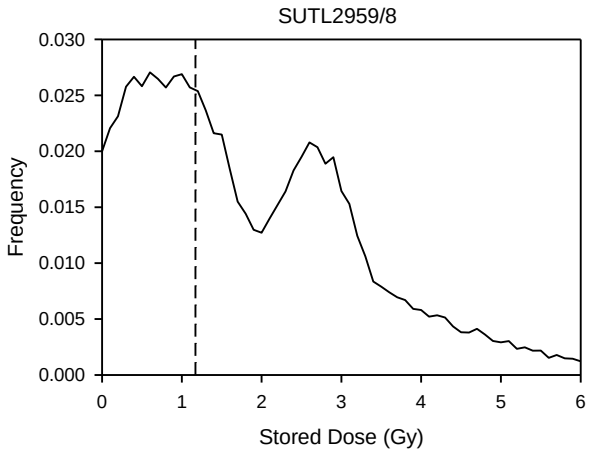

Figure D.16: Probability distribution plot for SUTL2959/8. The dashed line indicates the weighted mean.

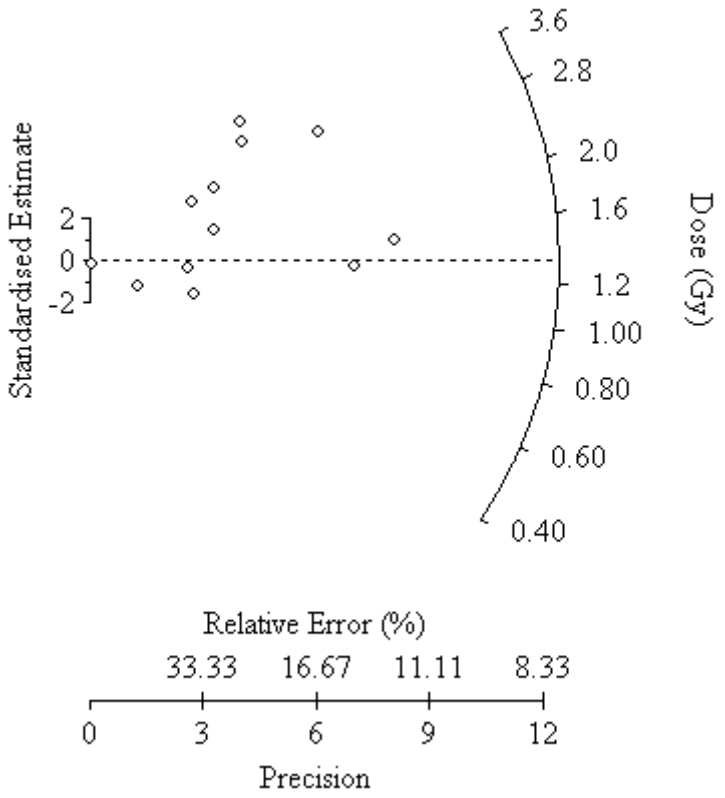

Figure D.17: Radial plot for SUTL2959/9. The dashed line indicates the weighted mean.

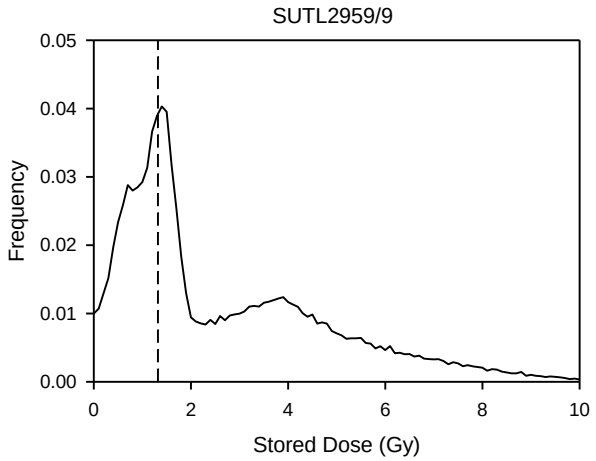

Figure D.18: Probability distribution plot for SUTL2959/9. The dashed line indicates the weighted mean.

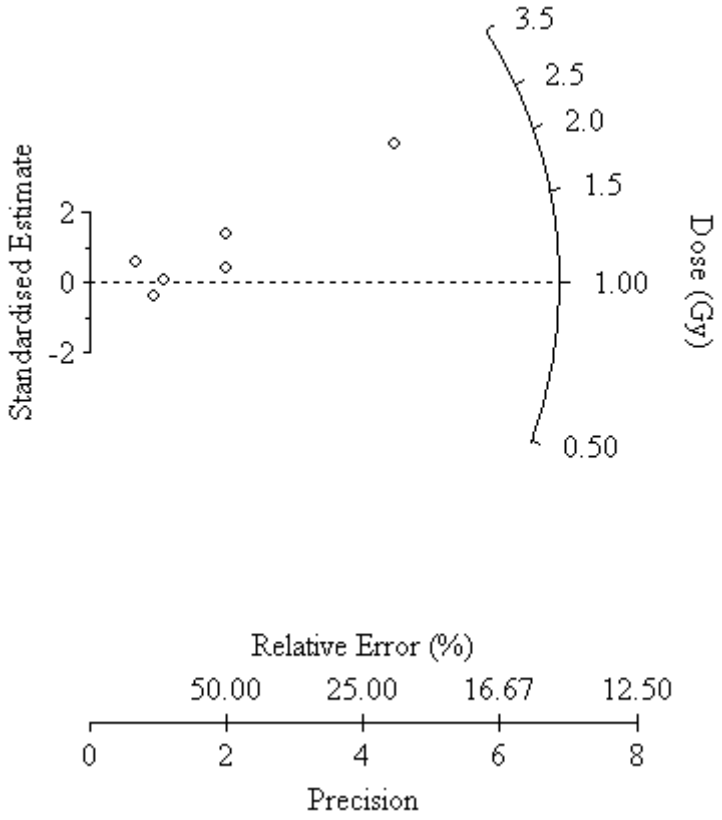

Figure D.19: Radial plot for SUTL2960/2. The dashed line indicates the unweighted mean.

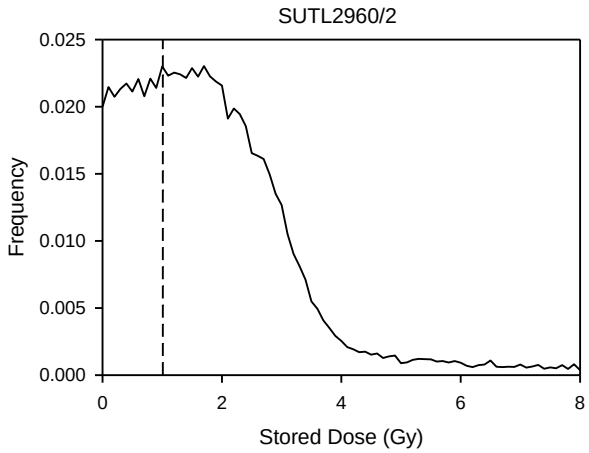

Figure D.20: Probability distribution plot for SUTL2960/2. The dashed line indicates the unweighted mean.

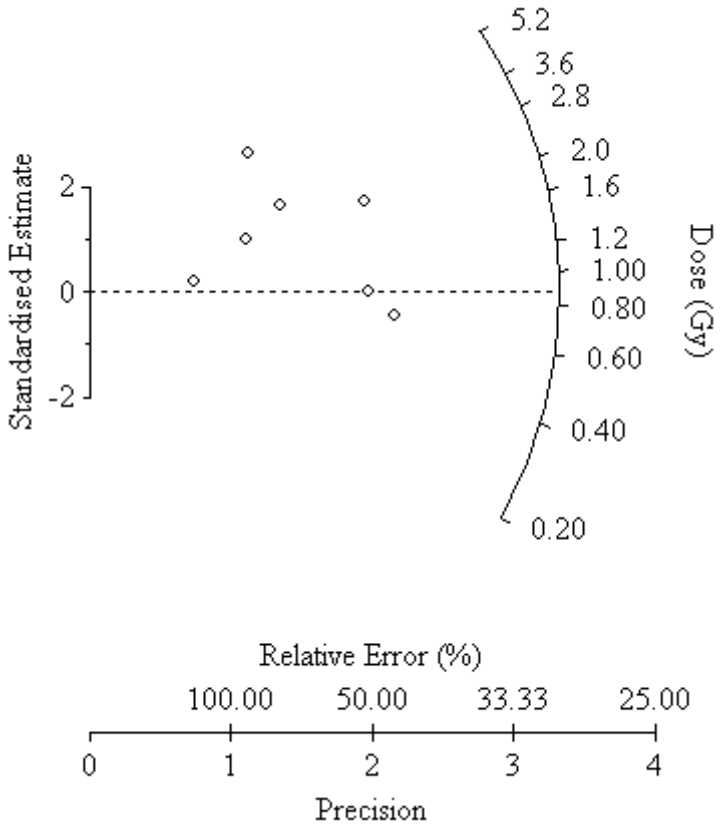

Figure D.21: Radial plot for SUTL2960/5. The dashed line indicates the weighted mean.

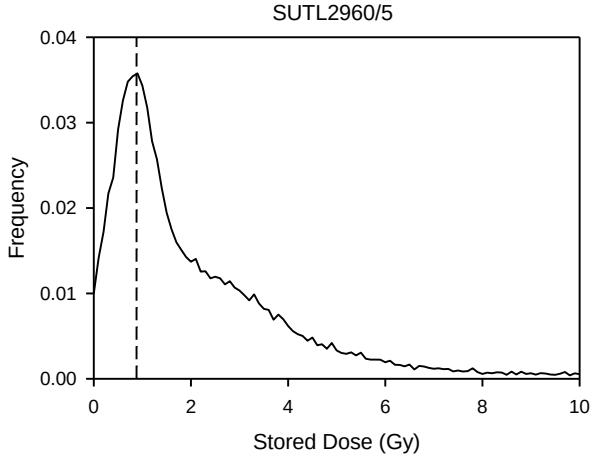

Figure D.22: Probability distribution plot for SUTL2960/5. The dashed line indicates the weighted mean.

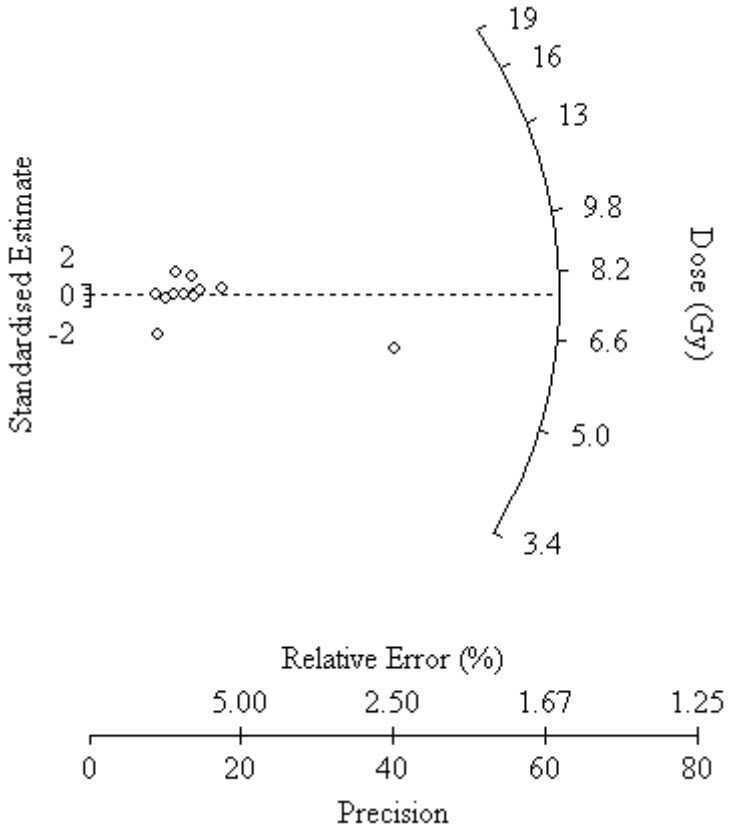

Figure D.23: Abanico plot for SUTL2960/15. The dashed line indicates the robust mean.

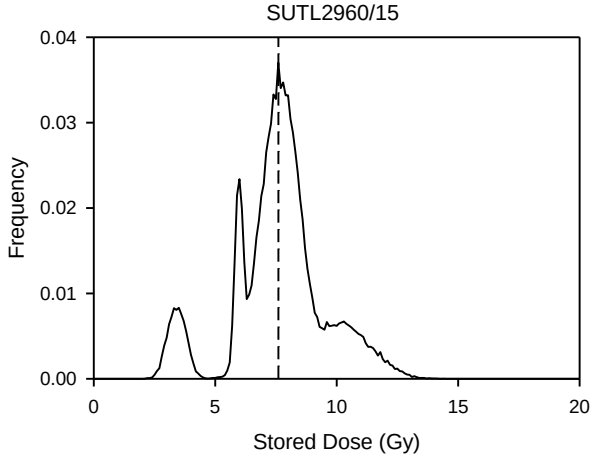

Figure D.24: Probability distribution plot for SUTL2960/15. The dashed line indicates the robust mean.

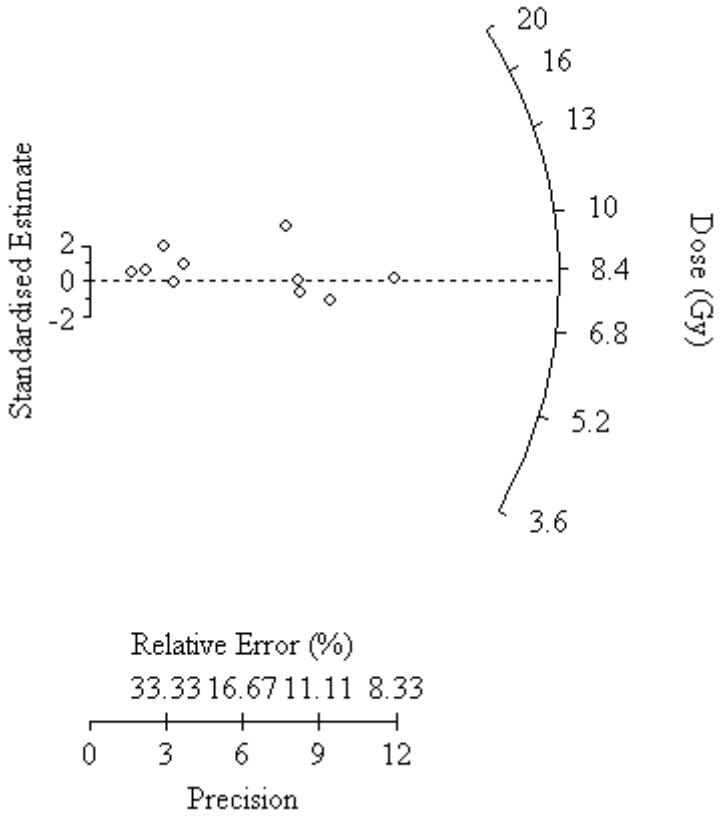

Figure D.25: Radial plot for SUTL2960/27. The dashed line indicates the weighted mean.

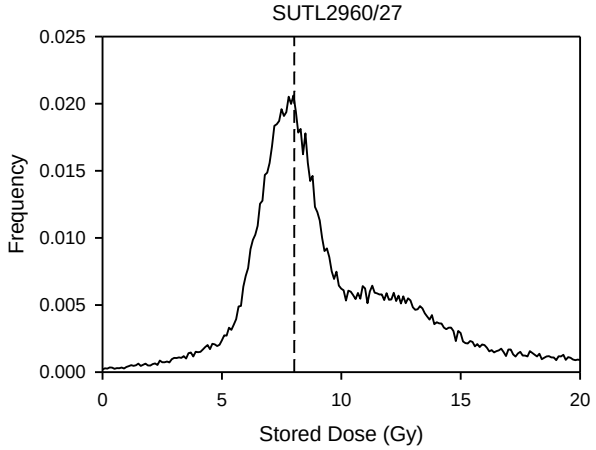

Figure D.26: Probability distribution plot for SUTL2960/27. The dashed line indicates the weighted mean.

Appendix E. Tabulated age-depth relationships

Sample	Depth (cm)	Dose rate (mGy a^{-1})	Profile measurements		SAR	
			Stored dose (Gy)	Apparent age (ka)	Stored dose (Gy)	Age (ka)
SUTL2959/1	15.5	3.71 ± 0.15	0.89 ± 0.11	0.24 ± 0.03	0.97 ± 0.17	0.26 ± 0.05
SUTL2959/2	35.5	3.53 ± 0.14	1.34 ± 0.15	0.38 ± 0.05	1.11 ± 0.25	0.31 ± 0.07
SUTL2959/3	54.5	3.40 ± 0.13	0.56 ± 0.03	0.16 ± 0.01	0.42 ± 0.10	0.12 ± 0.03
SUTL2959/4	74.5	3.26 ± 0.13	0.85 ± 0.11	0.26 ± 0.04	1.14 ± 0.12	0.35 ± 0.04
SUTL2959/5	92.5	3.62 ± 0.15	1.79 ± 0.74	0.49 ± 0.21	1.17 ± 0.09	0.32 ± 0.03
SUTL2959/6	111.5	3.60 ± 0.14	3.37 ± 0.59	0.94 ± 0.17	1.31 ± 0.11	0.36 ± 0.03
SUTL2959/7	132.5	3.55 ± 0.14	2.52 ± 0.37	0.71 ± 0.11	1.70 ± 0.67	0.48 ± 0.19
SUTL2959/8	151.5	3.60 ± 0.15	3.34 ± 0.32	0.93 ± 0.10	1.17 ± 0.15	0.33 ± 0.04
SUTL2959/9	171.5	3.60 ± 0.15	1.98 ± 0.21	0.55 ± 0.06	1.32 ± 0.10	0.37 ± 0.03

Table E.1: Dose rates, stored doses and ages for the profiling OSL measurements and SAR analysis of SUTL2959 (Lake Esmeralda).

Sample	Depth (cm)	Dose rate (mGy a^{-1})	Profile measurements		SAR	
			Stored dose (Gy)	Apparent age (ka)	Stored dose (Gy)	Age (ka)
SUTL2960/1	1	2.12 ± 0.07	0.54 ± 0.15	0.25 ± 0.07		
SUTL2960/2	2	**2.12 ± 0.07**	0.99 ± 0.19	0.47 ± 0.09	1.01 ± 0.35	0.48 ± 0.17
SUTL2960/3	3	2.15 ± 0.08	1.75 ± 0.31	0.81 ± 0.15		
SUTL2960/4	4	2.15 ± 0.08	0.70 ± 0.29	0.32 ± 0.14		
SUTL2960/5	5	**2.19 ± 0.08**	1.02 ± 0.28	0.47 ± 0.13	0.88 ± 0.25	0.40 ± 0.12
SUTL2960/6	6	3.30 ± 0.13	8.83 ± 0.64	2.68 ± 0.22		
SUTL2960/7	7	3.30 ± 0.13	10.19 ± 0.34	3.09 ± 0.16		
SUTL2960/8	8	3.30 ± 0.13	7.42 ± 0.23	2.25 ± 0.11		
SUTL2960/9	9	3.30 ± 0.13	8.19 ± 0.45	2.48 ± 0.17		
SUTL2960/10	10	3.30 ± 0.13	7.22 ± 0.39	2.19 ± 0.14		
SUTL2960/11	11	3.30 ± 0.13	7.30 ± 0.41	2.21 ± 0.15		
SUTL2960/12	12	3.30 ± 0.13	8.93 ± 0.36	2.71 ± 0.15		
SUTL2960/13	13	3.30 ± 0.13	8.17 ± 0.61	2.48 ± 0.21		
SUTL2960/14	14	3.30 ± 0.13	9.49 ± 0.46	2.88 ± 0.18		
SUTL2960/15	15	**3.30 ± 0.13**	9.78 ± 0.63	2.96 ± 0.22	7.60 ± 0.05	2.30 ± 0.09
SUTL2960/16	16	3.30 ± 0.13	9.42 ± 0.53	2.85 ± 0.20		
SUTL2960/17	17	3.30 ± 0.13	10.34 ± 0.52	3.13 ± 0.20		
SUTL2960/18	18	3.30 ± 0.13	9.27 ± 0.47	2.81 ± 0.18		
SUTL2960/19	19	3.30 ± 0.13	8.19 ± 0.29	2.48 ± 0.13		
SUTL2960/20	20	3.30 ± 0.13	7.99 ± 0.36	2.42 ± 0.14		
SUTL2960/21	21	3.30 ± 0.13	7.70 ± 0.39	2.33 ± 0.15		
SUTL2960/22	22	3.29 ± 0.12	8.50 ± 0.37	2.58 ± 0.15		
SUTL2960/23	23	3.29 ± 0.12	8.02 ± 0.50	2.44 ± 0.18		
SUTL2960/24	24	3.29 ± 0.12	9.46 ± 0.48	2.87 ± 0.18		
SUTL2960/25	25	3.29 ± 0.12	9.23 ± 0.42	2.81 ± 0.16		
SUTL2960/26	26	3.29 ± 0.12	8.06 ± 0.30	2.45 ± 0.13		
SUTL2960/27	27	**3.29 ± 0.12**	8.02 ± 0.27	2.44 ± 0.12	8.03 ± 0.38	2.44 ± 0.15
SUTL2960/28	28	3.29 ± 0.12	8.64 ± 0.19	2.63 ± 0.11		
SUTL2960/29	29	3.29 ± 0.12	5.65 ± 0.21	1.72 ± 0.09		
SUTL2960/30	30	3.29 ± 0.12	6.94 ± 0.21	2.11 ± 0.10		
SUTL2960/31	31	3.29 ± 0.12	7.50 ± 0.17	2.28 ± 0.10		

Table E.2: Dose rates (measured values in bold, other values interpolated from these), stored doses and ages for the profiling OSL measurements and SAR analysis of SUTL2960 (Monolith Lake).